UNIVERSITÀ DEGLI STUDI DI PADOVA
DIPARTIMENTO DI FISICA E ASTRONOMIA

CORSO DI LAUREA TRIENNALE IN ASTRONOMIA

The history of star-formation in galaxies

Valeria Politino

Supervisor: Prof. Alberto Franceschini

Contents

Chapter 1

Introduction

The problem of measuring the history of star-formation has always been a crucial one in cosmology. A lot of different techniques have been developed over the years, and this thesis aims to review the most important literature on the subject of star-formation in galaxies, resume its results and also give a brief outlook on the future of the observations in this field. The thesis is structured as follows: in Chapter 2 the star-formation rate (SFR) indicators will be examined (namely UV, far infrared -FIR- and radio light, then in Chapter 3 the present estimates of the SFR from UV and FIR observations will be presented, along with a special focus on the samples which these estimates are based on. In Chapter 4 radio data will be analyzed; Chapter 5 will instead focus on the sub-millimetric observations. Finally, the last chapter will cover the issue of future developments in bettering the current estimates.

1.1 The Lilly-Madau plot

One of the very first modern SFRD measurements were done by Lilly et al. (1995) and by Madau et al. (1996), who then in 2014 thoroughly collected all the techniques and tools used in the measurements of the SFRD(z) (Madau & Dickinson (2014)). The assumptions made in his work are a universal initial mass function (IMF), correction for dust absorption and a classic hierarchical view for the formation of galaxies. The latter is a simplification, as we know that more complex processes are involved in the formation of galaxies, but it is a useful approximation. They measured the SFRD(z) in many ways:

- The UV light emitted in the continuum ($1400\,\mathring{A} < \lambda < 1700\,\mathring{A}$); this is because the UV-light characterizes short-lived massive stars, namely young stars. Although it may seem a good tracer for SFRD(z), it is important to consider dust attenuation, which has an important effect

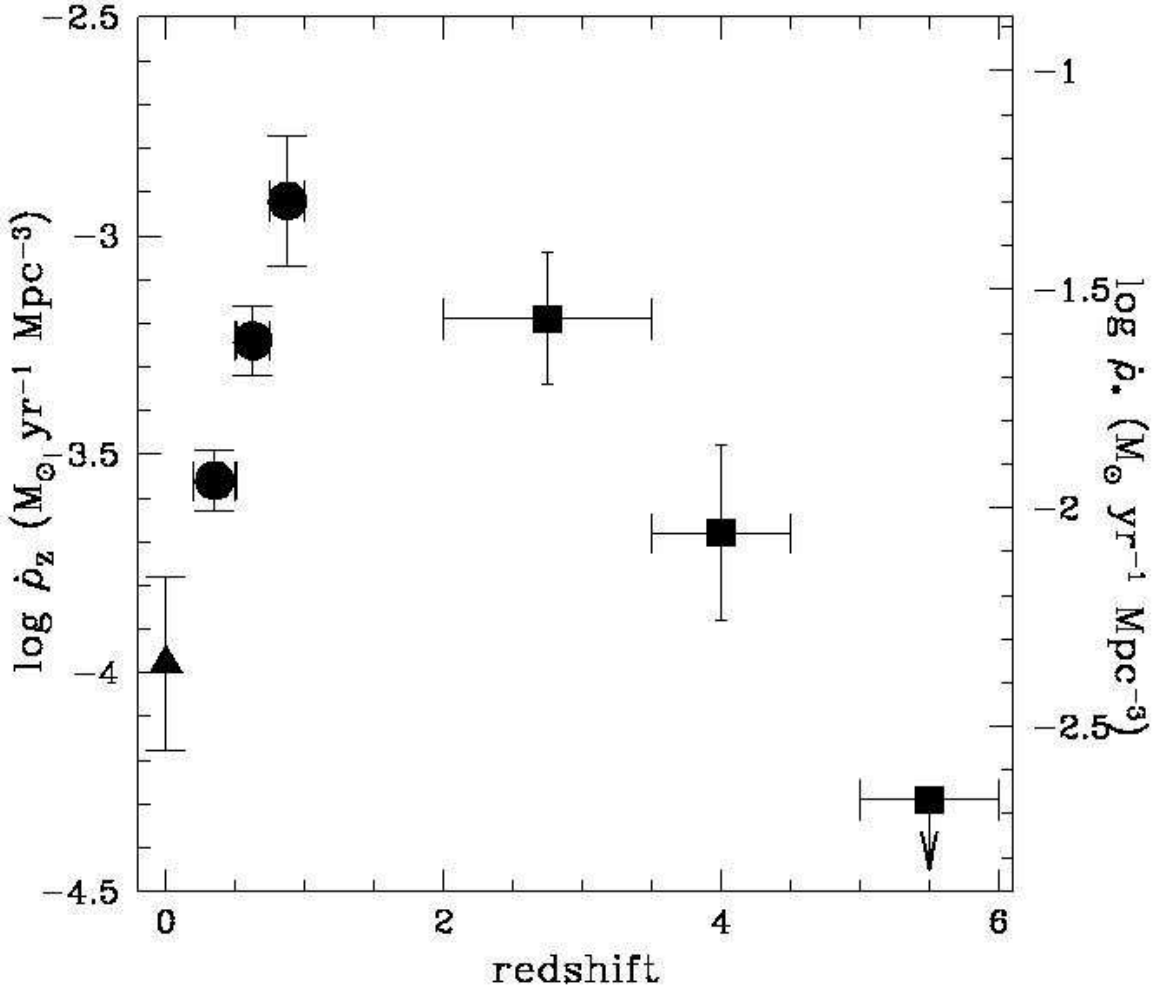

Figure 1.1 The star-formation history of the universe, from the first study of Madau (Madau et al. (1996)). A more accurate graphic with most recent data will be presented in Chapter 3.

at these wavelenghts. The relationship between UV light and SFR is a linear one:

$$SFR = K_{FUV} * L_\nu(FUV) \tag{1.1}$$

where $L_\nu(FUV)$ is the specific far UV luminosity ($erg\,s^{-1}\,Hz^{-1}$) and K_{FUV} is a conversion factor that depends on the history of star-formation, metallicity, IMF and the exact FUV wavelength. Assuming a Salpeter IMF (Salpeter (1955)) within a mass range from 0.1 to 100 $M_\odot$ and a constant SFR, from the photometric models of Conroy (Conroy et al. (2009)) it follows $K_{FUV} = 1.26 * 10^{-28}$ as a mean value.

- Knowing that UV light is absorbed by dust and then re-emitted at infrared (IR) wavelengths, MIR and FIR light give another good tracer for the SFR. It is however important to discard the sources of IR light not related to star formation. The relationship is similar to the previous one:

$$SFR = K_{IR} * L_\nu(IR) \tag{1.2}$$

- The comoving stellar mass density (SMD) that can be traced from NIR light can be used to trace SFR, because it is mainly due to near-solar-mass evolved stars that account for most of the galactic stellar mass.

- The Core-Collapse Supernova Rate is also a potentially good tracer, but it has many downsides such as poor statistics and dust attenuation.

We have briefly mentioned some of the problems that affect the measurement of the SFR; now we will account for them more specifically, even though some of them will be examined with the pertinent data in the following chapters.

- **The initial mass function.** The IMF is an empyrical function that gives the distribution of masses in a stellar population at the epoch of formation. It gives the ratio between hot, bright stars that dominate the light and cool, faint stars that dominate the mass. Consequently, it controls the evolution (both in luminosity and in color) of a stellar population, as stars with different masses evolve at different rates. Some constraints are needed to infer the IMF: the mass is usually inferred from the light, but the mass to light ratio (M/L) is needed, and it depends on the age of the stellar population, on the history of star-formation and on the presence of dust. The latter in particular could be a crucial factor in underestimating the mass, because the stellar counterpart is simply not visible. Furthermore, the conversion from light to mass is not straightforward, but population synthesis models are needed, and their reliability is not certain as a matter of fact. These data can be directly inferred only for nearby galaxies - so it is possible to construct a model for the IMF based on these. The most

popular one is the simple power-law Salpeter IMF (Salpeter (1955)), generally truncated over a finite mass range ($0.1\,M_\odot - 100\,M_\odot$); it is widely used, but, as we will see in Chapter 3, the choice of a Chabrier IMF could be more reliable.

- **Dust attenuation.** We have already mentioned how the presence of dust can affect the measurements: it yields an underestimation of the mass for the IMF, it absorbs the UV light thus compromising the reliability of the latter as a star-formation tracer, and so on. Many have tried to model the dust attenuation assuming a universal attenuation curve; however, many studies pointed out how the attenuation law can change in a non-negligible way from galaxy to galaxy, making it very difficult to estimate the dust absorption very effectively.

- **Data and redshift bins.** It is not possible to have a complete data set for a wide redshift range: in fact, different surveys cover different redshift ranges. Up to $z = 1$, the sample is complete and not dramatically affected by dust of star-forming regions, even though we cannot neglect the presence of interstellar medium (ISM). From $z > 2$, and especially from $z > 4$, the sample becomes incomplete and only hyperluminous sources are visible.

Chapter 2

Star-formation rate indicators

In this chapter the main star-formation rate tracers will be examined, with a special focus on fundamental characteristics and intrinsic flaws of each, namely UV light, IR light and radio emission. Measuring the SFRD means deriving the mass from light; this is affected by the mass to light (M/L) ratio, which depends on age, star-formation history (SFH) and extinction: high M/L ratios are typical of passively evolving, old stellar populations, while young, unreddened and actively star-forming galaxies show low M/L ratios. The conversion from light to mass is made through population synthesis models, which compute the predicted spectrum of a galaxy based on its properties. However, this is a difficult task, because for most galaxies the only observable quantity is the integrated light, which is a sum of many effects derived from the true distribution of properties of that stellar population, often unkown. Different processes have similar effects on the spectrum: for example, age, metallicity and dust attenuation all contribute to a reddening effect. These degeneracies can only be partially resolved: this is the reason why simplifying assumptions are needed, like those concerning the universal IMF, as we saw in the Introduction.

2.1 UV light

It has already been mentioned how the UV-continuum emission is dominated by short-lived massive stars; this means that, given a specific IMF and accounting for the dust content that absorbs part of the emission (effect that is often severe), it is a direct measure of the star-formation rate density (SFRD). Young stars (which dominate the UV emission) have very short lifespans. For a Salpeter IMF, the 1500 $\mathring{A}$ luminosity of a simple stellar population (SSP) fades by a factor of 100 after 10^8 years, and by factors from 10^3 to 10^6 after 10^9 years, depending on the metallicity. This means

that, bolometrically, at least half of the luminous energy of a SSP emerges in the first 10 Myr, making this a natural wavelength to measure the SFR. For a galaxy forming stars at a constant rate, the 1500 $\mathring{A}$ luminosity stabilizes once O-stars evolve off the main sequence. For solar metallicity, by an age of $10^{7.5}$ years, it has reached 75% of its asymptotic value. For these reasons, the UV luminosity at wavelengths of $\sim 1500\,\mathring{A}$ (wavelengths from 1400 $\mathring{A}$ to 1700 $\mathring{A}$ have been used for both local and high redshift studies) is regarded as a good tracer of the formation rate of massive stars. However, measurements at low redshifts (namely, $z \lesssim 1.4$) can be done only through space-based UV data or are limited to longer UV wavelengths. Mid-UV reference wavelengths that have been used in the literature include 2300 $\mathring{A}$ and 2800 $\mathring{A}$. The mid-UV emission from a galaxy can have a larger contribution from longerlived, lower-mass stars, particularly at later ages, and the time evolution of the luminosity is more gradual, particularly after $\sim$ 250 Myr, when the 1500 $\mathring{A}$ luminosity of an SSP drops off sharply, while the 2800 $\mathring{A}$ luminosity continues to fade at an approximately exponential rate. This complicates the conversion from luminosity to SFR, as well as any correction for dust extinction based on the UV spectral slope. Besides, the effect of the metallicity is not neglectable: less-metal-rich stars produce more UV light, so we expect variations in the FUV luminosity with the evolution of the metallicity in a galaxy.
We already saw how the conversion between the intrinsic FUV-specific luminosity $L_\nu(FUV)$ (in units of $erg\,s^{-1}\,Hz^{-1}$) corrected for extinction and the SFR ($M_\odot\,year^{-1}$) is made:

$$SFR_{UV} = K_{FUV} * L_\nu(FUV) \tag{2.1}$$

For a Salpeter IMF in the mass range $0.1-100 M_\odot$ and constant SFR, the flexible stellar population synthesis (FSPS) models (Conroy et al. (2009)) yield $K_{FUV} = (1.55, 1.3, 1.1, 1.0) * 10^{-28}$ for $logZ_*/Z_\odot = (+0.2, 0, 0.5, 1.0)$ at age $\gtrsim 300 Myr$. In this work, a constant FUV conversion factor $K_{FUV} = 1.15 * 10^{-28}\,M_\odot\,year^{-1}\,erg^{-1} sHz$ is adopted. For a detailed review of the conversion factor, see Madau & Dickinson (2014).

2.2 IR light

The IR light has two components which the star-formation activity can be measured through:

- The near infrared light (NIR) is dominated by near-solar-mass evolved stars that form the bulk of a galaxy stellar mass; this yields therefore a direct source for the comoving stellar mass density (SMD);
- The far infrared light (FIR) is instead dominated by the re-emission of UV light in dusty regions, therefore accounting for the lost emis-

sion in the UV measurements. Dust absorption at IR wavelengths is considered negligible.

The uncertainties that must be taken into account are several: for example, AGNs can be a source of UV light absorbed and re-emitted in IR, and older stellar population can heat the dust in their surroundings, thus contributing to IR emission. However, for very actively star-forming galaxies without AGN it is assumed that most of the IR emission comes from star formation processes. A galaxy's total IR luminosity should be measured by fitting a dust emission model to observations at several wavelengths. Unfortunately, such multiwavelength data are often unavailable, and a SED, often derived from observations of local galaxies, is used to extrapolate the total L_{IR} from a single observed flux density at some MIR or FIR wavelength. Thus, the derived SFRs can be affected by strong variations in the dust emission properties of each galaxy. The spectrum of dust emission is rather complex: most of the dust mass in a galaxy is usually in the form of relatively cold dust $(15 - 60\,K)$ that contributes strongly to the emission at FIR and submillimeter wavelengths $(30 - 1000\,\mu m)$. Dust can be present at different temperatures, with colder grains in the ISM and warmer ones in star-forming regions. The MIR spectral region $(320\,\mu m)$ is very complex: it has strong emission bands from polycyclic aromatic hydrocarbons and absorption bands from silicates. AGN may contribute to strong continuum emission from warm dust, and can dominate over star-formation at MIR wavelengths. In the FIR, however, their role is less prominent.
In analogy with Equation 2.1, we have defined:

$$SFR_{IR} = K_{IR} * L_{\nu}(IR) \tag{2.2}$$

where $L_{\nu}(IR)$ is the IR luminosity integrated over the wavelength range from 8 to 1000 μm and K_{IR} is once again derived using FSPS from Conroy et al. (2009), with an assumed value of $K_{IR} = 4.5 * 10^{-44}\, M_{\odot}\, year^{-1}\, erg^{-1}\, s$ (Madau & Dickinson (2014)). We already mentioned how the contribution of AGNs and older stars can affect IR measurements; it must also be taken into account that if the dust opacity is not so large and a significant amount of UV radiation emerges, then the SFR derived from the IR luminosity will be biased. Accounting for dust absorption is no easy task: in general, different relative distributions of stars and dust can lead to different net attenuation properties. Winds from star-forming regions can blow away dust on certain timescales, whereas other regions that are younger or more deeply covered by the galaxy's ISM remain more heavily obscured. Dust heating also depends on geometry, leading to different distributions of dust temperatures and different emission spectra at IR and submillimeter wavelengths. For a more detailed study of dust extinction laws, see Madau & Dickinson (2014).

2.3 Radio emission

Radio emission has been recently used as a star-formation tracer, as SN-accelerated electrons emit non-thermal (synchrotron) radiation at centimeter wavelengths, produced by ultrarelativistic electrons (with Lorentz factors $\gamma \gg 1$) spiraling around magnetic field lines; this is directly linked to type II and Ib core-collapse SNe explosions, thus taking into account only high-massive, very bright, young stars. In fact, when massive stars undergo supernova explosions, the expanding remnants can accelerate the cosmic ray electrons thus bringing up synchrotron radiation, which dominates the radio emission at rest-frame frequencies $< 30\,GHz$. Another source of synchrotron emission can be the ejection of relativistic jets of plasma from supermassive black holes. Thermal (free-free) emission from electron-ion Coulomb interactions in HII regions can also contribute, particularly at higher frequencies ($> 5\,GHz$), giving a direct view on star-forming regions.
A remarkably tight correlation (infrared-radio correlation - IRRC - see Delhaize et al. (2017a)) is observed between radio emission and FIR emission in local galaxies spanning many orders of magnitude in luminosity: this is used to calibrate the SFR for radio luminosities, and the empyrical correlation holds up to $z < 2$, but it is likely that it is still valid up to $z \lesssim 5$. Even though several theoretical models have attempted to explain the exact mechanism and processes that regulate the IRRC, none of them have successfully completed this task. A general idea is given from the fact that the energy absorbed by dust grains after a SN explosion is then re-radiated as thermal emission in the IR.
Radio emission is free from dust extinction and it can be detected at large cosmic distances, thus offering a relatively unbiased tracer of star formation. Radio-detected galaxy populations are of two kind: star-forming and AGN galaxies; furthermore, the latter population also splits up in two categories that can be classified through the host galaxies' optical spectroscopic emission line properties as high- and low- excitation radio AGN. High-excitation AGN have green optical colours and they are hosted in a galaxy where a supermassive black hole is accreting radiatively efficiently from a geometrically thin, but optically thick accretion disk. Instead, low-excitation one are found in massive, red, quiescent galaxies and they do not show the classical properties of a unified-model AGN, unlike the former one, because they are thought to have a geometrically thick but optically thin disk and a different accretion process. For their radio emission exceeds the level expected from star-forming activity, they are called radio-loud objects (and they are a minority population). It is important to discard these sources for the final estimate of the SFR, and we will see how this goal is reached in Chapter 4. Radio emission should also be suppressed at earlier cosmic epochs, as electrons would lose energy by inverse Compton scattering off microwave background photons whose energy density increases at high redshift.

From observation and evolutionary models (see Novak et al. (2017)), it is known that star-forming galaxies dominate the faint end of the radio counts and have strongly luminosity functions; therefore, deep surveys are needed in order to have a clear view of the evolution of this population. As we will see in Chapter 4, the VLA-COSMOS 3 GHz project will suit this task perfectly, it being the up-to-date deepest radio continuum survey over a relatively large field.

Chapter 3

Current SFR estimates based on UV and FIR

In this chapter the current consensus on the SFRD based on UV and IR data will be examined, starting from a brief presentation of the surveys whose data have been used and then reviewing techniques and results that have been found. For a detailed and thorough collection of every survey and study that has been analyzed, see Madau & Dickinson (2014).

3.1 Observations. The samples

3.1.1 UV surveys

The first modern SFRD measurements were done in the Canada-France Redshift Survey (CFRS) by Lilly et al. (1995). They had the credit to first combine a large and deep spectroscopic redshift survey with multiwavelength photometry and to derive LFs and luminosity densities at several different rest-frame wavelengths, including the rest-frame UV. This survey used the 4-m Canada-France-Hawaii Telescope and mainly surveyed the Universe out to $z < 1$. They made direct measurements of 2800 $\mathring{A}$ rest-frame luminosities at $z > 0.5$ through BV IK-band photometry, and down to $z \approx 0.3$ with modest spectral extrapolation. They found that the 2800 $\mathring{A}$ luminosity density declined by approximately one order of magnitude from $z = 1$ to the present, which was interpreted as a steep decline in the SFRD.

Madau et al. (1996) extended this analysis to higher redshifts through the Hubble Deep Field observations (HDF). They used color-selected Lyman break galaxies (LBG, a UV-selected population of star-forming high-redshift galaxies) samples at $\langle z \rangle = 2.75$ and 4. The deep HST WFPC2 photometry allowed luminosities to be measured at 1500 $\mathring{A}$ in the rest-frame, reaching fainter than contemporaneous ground-based LBG data. Madau et al. (1996) inferred only lower limits for the SFRD, without extrapolation to fainter

luminosities and without correction for dust absorption. Later analyses followed to extrapolate total UV luminosity densities and improve photometric redshift analyses (see Madau & Dickinson (2014) for better information); all these studies (with the HDF measurements at $z > 1$ and the CFRS measurements at $z < 1$) suggested a general rise and fall picture of a UV luminosity density and, consequently, the cosmic SFH that peaked somewhere between $z \approx 1$ and 2. Several studies in the following years have confirmed and extended this analysis, usind Hubble Deep Field (HDF) data or deeper spectroscopic surveys with the Keck telescope.
UV rest-frame observations at $z < 1$ should be done from space telescopes to reach shorter UV wavelengths than those used in the ground-based studies. The most cited analysis that covers this redsfhift bin is from Arnouts et al. (2005), who combined deep GALEX observations with spectroscopy from the VIMOS VLT Deep Survey (VVDS), thus deriving 1500 $\mathring{A}$ rest-frame luminosity functions at $0.2 < z < 1.2$; that said, it is important to remark that they used only only $\sim$ 1000 galaxies with spectroscopic redshifts over the whole range $\Delta z = 1$ in a single field covering $0.5\, deg^2$, which can be subject to cosmic variance related problems. The LFs derived in this study will be confirmed by Cucciati et al. (2012), who analyzed a larger, deeper and more complete spectroscopic sample in the same VVDS survey field studied by Arnouts et al. (2005). The most recent and robust data, however, comes from spectroscopy data collected with the Keck telescope of LBGs, covering many sightlines thus minimizing any cosmic variance effect. The best LF analysis is made by Reddy et al. (2008), who had the merit to achieve a degree of spectroscopic confirmation and calibration for higher galaxies never reached before, even still relying on photometric color-selected samples to probe the faint-end of the LF. At higher redshifts, $4 < z < 7$, the most important source of data are deep HST observations; in fact, after the installation of the Advanced Camera for Surveys (ACS), it has been possible to provide better optical imaging in wider fields than the original HDF; it also bettered the sensitivity of the telescope at redder wavelengths, making Lyman-break selection possible up to $z \approx 6$. The two most important surveys which provided data to infer the SFRD are the Great Observatories Origins Deep Survey (GOODS), which provided a sample of several thousand Lyman-break candidates at $z \approx 4$ and around 1000 at $z \approx 5$, and the Hubble Ultra Deep Field (HUDF), which observed a single ACS pointing ($\sim 11\, arcmin^2$) with very long exposure times, reaching fainter objects than the original HDF and with better sensitivity at higher redshifts. The first analyses of the GOODS data brought up relatively mild evolution of the UV luminosity density from $2 < z < 5$ and evidence that there were fewer high-luminosity galaxies at $z \approx 6$. Later on, these conclusions have been revised by following studies that used deeper data and more rigorous analyses, demonstrating that the UV-LF evolves significantly at $z > 4$. The current accepted hypothesis is that this is primarily luminosity evolution, at least at

$4 < z < 7$, which yields the consequence that the number density of bright LBGs increases rapidly with time, more quickly than does the integrated luminosity density. Further analyses point to a luminosity evolution up to $z \sim 8$, although secure spectroscopic information becomes possible only for few galaxies at this redshift. They also examined the faint-end slope of the LF, measuring very steep values, in some cases approaching or exceeding the divergent value $\alpha = 2$. There is broad agreement that UV spectral slopes for LBGs are bluer at $z > 4$ than at lower redshifts, which has consequences for their dust extinction and total SFRD. Several studies have also tried to extend SFRD analyses to $9 < z < 12$, using data from the HUDF or from gravitationally-lensing cluster studies. Although robust data are still missing, these measurements have their main importance in focusing on the earliest phases of galaxy evolution and on the reionization of the IGM, but their impact on the global star-formation budget of the Universe is not remarkable, given that, according to the current estimates, only $\sim 1\%$ of the cosmic comoving SMD present today was formed at $z > 6$.

3.1.2 IR surveys

The first studies on the SFRD through IR data has been made thanks to the Infrared Astronomical Satellite (IRAS), through which measurements of local FIR luminosity functions (FIRLF) have been possible since 1986, when the first study on the subject has appeared (Lawrence et al. (1986), but a lot more have followed throughout the years). The typical observation wavelength was $60\,\mu m$, otherwise FIR luminosities integrated over a broader wavelength range have been used. They were also generally extrapolated from the measured IRAS fluxes using fitting methods. We consider L_{IR} as the total luminosity integrated over the range $8 - 1000\,\mu m$, which includes most of the bolometric luminosity of dust emission from sources of interest. After IRAS, which has $100\,\mu m$ as longest wavelength band, AKARI extended this threshold up to $160\,\mu m$ to provide more reliable measurements of the bolometric luminosity and reduce bias against galaxies with cold dust temperatures.

The bright end of the IRLF is dominated by galaxies with warmer dust temperatures, which tend to be starburst galaxies and dusty AGN. Nearly all studies found out that it cuts off less sharply than does the exponential one used in the Schechter function. Furthermore, several studies have measured a steep faint-end slope α ($dN/dL \propto L^{\alpha}$), such as $\alpha = 1.6$ (Sanders et al. (2003)), but other studies have found much flatter distributions: this means that the faint-end has not been well-sampled and it is an issue that need further betterment.

It is believed that in relatively quiescent galaxies more than half of the FIR luminosity is due to the emission from dust in the general ISM heated by ambient starlight, thus not being linked to star-formation activity: this

could mine the reliability of FIR light in effectively trace the SFR. We may expect that this problem becomes less remarkable at higher redshifts, when specific SFR of typical galaxies was much larger and the net dust extinction to star-forming regions was, on average, larger; but in reality we do not know the effective impact of intermediate-age stars even at higher redshifts. The first deep IR surveys were made with ISO (Franceschini et al. (2001), Elbaz et al. (2002)), but they covered a small sample of galaxies mainly at $z \leq 1$, so it was difficult to extrapolate reliable LFs from those data. The first big step forward was the Spitzer telescope, which enhanced the sensitivity and the area of deep IR observations; also very large spectroscopic redshift surveys had become available at that time and photometric redshift techniques were much bettered. Le Floc'h et al. (2005) made an analysis of $24\,\mu m$ sources at $0.3 < z < 1.2$ in the Extended Chandra Deep Field South. Integrating over derived IRLFs, they inferred an evolution of the IR luminosity density $\propto (1+z)^{3.9\pm0.4}$, much more steeper than the evolving UV luminosity density, $\rho_{FUV} \propto (1+z)^{2.5}$ (Schiminovich et al. (2005)). Furthermore, the fraction of the IR luminosity density produced by LIRGs and ULIRGs evolved even more steeply: Le Floc'h et al. (2005)) found that galaxies with $L_{IR} > 10^{11}\,L_{\odot}$ produced $70\% \pm 15\%$ of the IR luminosity density at $z \approx 1$ (compared with $5-15\%$, value of the current cosmic epoch); the oscillation depends on the adopted local LF.

At higher redshifts, instead, the available data rarely constrain the slope of the LF at the faint end; most analyses are forced to assume a faint-end slope based on measurements at lower redshifts, thus making them subject to large uncertainties in the extrapolations to total IR luminosity densities. There are more factors that can affect the extrapolation: or example, the SED templates adoptes, or procedures to account for AGN emission (see Rodighiero et al. (2010)).

An important study by Gruppioni et al. (2013) on Herschel data sets in the GOODs fields has brought up the most reliable results: they found that the characteristic luminosity L^*_{IR} continued to brighten even at $z > 2$, even though at a slower rate. Being not able to measure directly the faint-end slope of the IRLF at high redshift, they fixed it to a value derived locally ($\alpha = 1.2$). They find evolution by a factor of ~ 6 between $z = 1.1$ and today and relatively flat evolution at higher redshift to $\langle z \rangle = 2.75$.

3.2 Results

Let us now compare recent determinations of the IRLFs and UVLFs at $0 < z < 4$. The UVLFs in Figure 3.2 show the observed luminosities uncorrected for extinction, and are presented in units of solar luminosities (for a more direct comparison with the IRLFs).

There are many points that indicate low extinction for galaxies with

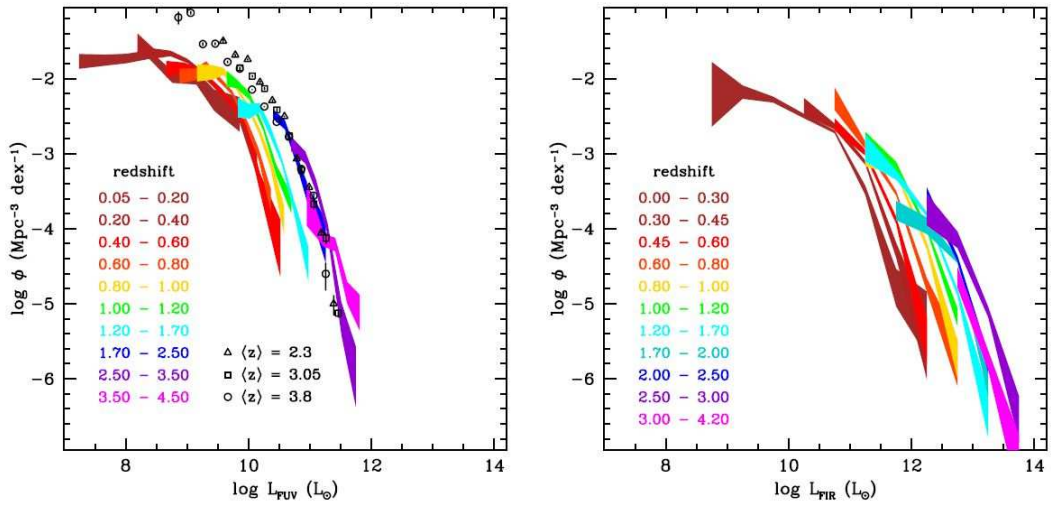

Figure 3.1 (*Left panel*) From Cucciati et al. (2012): redshift evolution of the FUV luminosity function at $0 < z < 4$. The colored bands indicate the 68% confidence intervals on the space densities over the observed luminosities (uncorrected for dust attenuation), in different redshift ranges. Data points, coded by shape, show the FUV luminosity functions for LBGs at mean redshifts $\langle z \rangle = 2.3$ and $\langle z \rangle = 3.05$. These luminosity functions use color selection techniques to extend the measurements to fainter luminosities than those measured in the purely spectroscopic samples from Cucciati et al. (2012). The FUV luminosity functions at $2. < z < 3.8$ are observed to be quite similar. (*Right panel*) Redshift evolution of the FIR luminosity function at $0 < z < 4$ from Gruppioni et al. (2013). The bands indicate the 68% confidence intervals at each redshift.

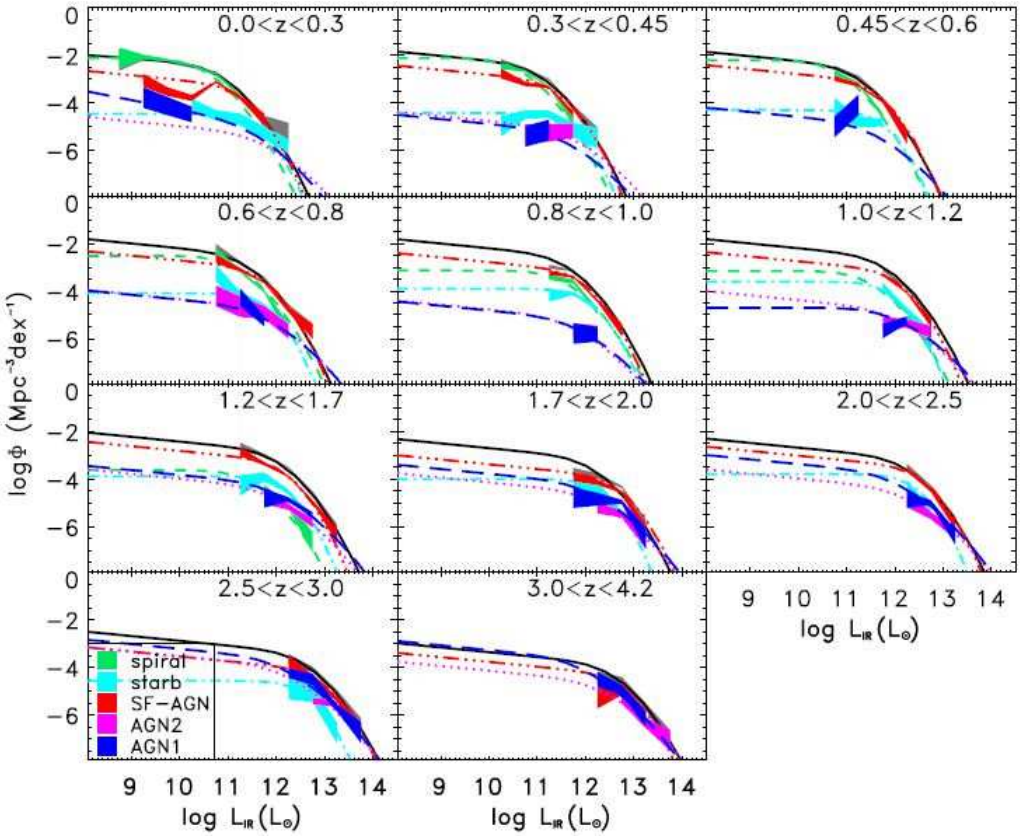

Figure 3.2 From Gruppioni et al. (2013): Total IR Luminosity Function estimated with the $1/V_{max}$ method by combining the data from the four PEP fields for the different populations (their $\pm 1\sigma$ uncertainty regions are shown as coloured filled areas: green for spirals; cyan for starbursts; red for SF-AGN; magenta for AGN2; and blue for AGN1), compared to the total LF ($\pm 1\sigma$, grey filled area). The best-fit modified Schechter functions are also plotted, extrapolated to fainter and brighter luminosities than covered by the data (with the black curve being for the total LF and the same colours used for the filled areas as for the single populations).

lower SFRs and a significant contribution from low-luminosity galaxies to the global SFRD at high redshift:

- The IRLFs cut off less steeply at high luminosities than the UVLFs;
- At the same redshifts, it is clear that the IRLFs extend to higher luminosities than the UVLFs: this is directly connected to the fact that actively star-forming galaxies are heavily dust-obscured;
- There is strong luminosity evolution, more for the IRLFs than the UVLFs;
- As we have already seen in section 3.1.1, the UVLFs (from Cucciati et al. (2012)) tend to have steeper faint-end slopes at higher redshifts, particularly for $z > 2$.

Madau et al. (1996) developed a method to derive the SFRD $\psi(t)$ directly from galaxy surveys by coupling the equations of chemical evolution to the spectrophotometric properties of the cosmic volume under consideration. The specific luminosity density at time t of a cosmic stellar population characterized by an SFRD $\psi(t)$ and a metal-enrichment law $Z_*(t)$ is given by the convolution integral:

$$\rho_\nu(t) = \int_0^t \psi(t-\tau) L_\nu[\tau, Z_*(t-\tau)] d\tau \tag{3.1}$$

where $L_\nu[\tau, Z_*(t-\tau)]$ is the specific luminosity density radiated per unit initial stellar mass by a SSP of age τ and metallicity $Z_*(t-\tau)$.
In deriving a SFR from a luminosity function it is necessary to provide best-fit LF parameters - generally Schechter functions for the UV data, but other functions for the IR measurements. Thus it becomes possible to integrate the LF down to the same relative limiting luminosity, in units of the characteristic luminosity L^*. In the following analysis, an integration limit $L_{min} = 0.03\,L^*$ is adopted when computing the luminosity density. For a Schechter function:

$$\rho_{UV}(z) = \int_{0.03L^*}^{\infty} L\phi(L,z) dL = \Gamma(2+\alpha, 0.03)\phi^* L^* \tag{3.2}$$

where α is the faint-end slope of the Schechter parameterization, and Γ is the incomplete gamma function.
Using Equations 2.1 and 2.2, it is possible to obtain measurements of the observed UV and IR SFRDs (see Figure 3.3). Given that the UV data are not corrected for dust extinction, it is clear that the gap between the UV and IR measurements increases with redshift up to at least $z \approx 1$ and then may narrow from $z = 1$ to 2.

It is evident that a robust estimate of dust attenuation is crucial to transform FUV luminosity densities into total SFRDs. Figure 3.3 shows

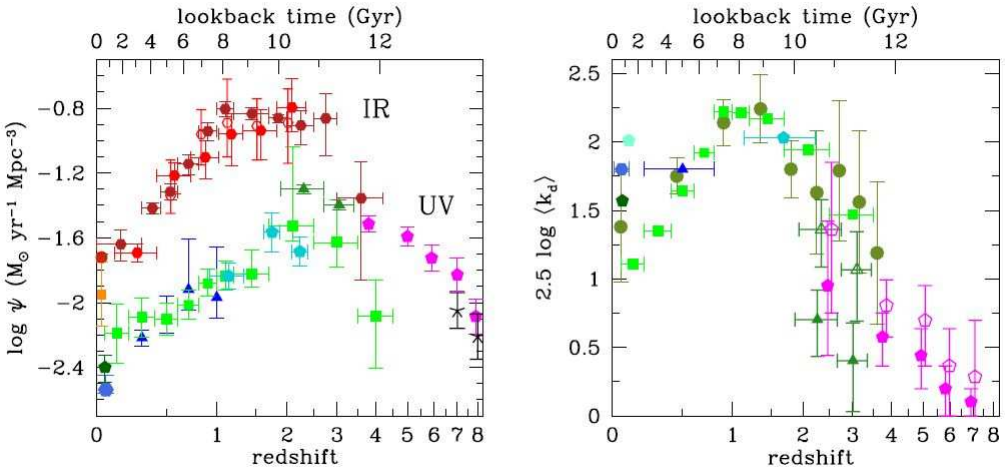

Figure 3.3 From Madau & Dickinson (2014): (*Left panel*) SFR densities in the FUV (uncorrected for dust attenuation) and in the FIR. All UV and IR luminosities have been converted to instantaneous SFR densities using the factors $K_{FUV} = 1.15 * 10^{28}$ and $K_{IR} = 4.5 * 10^{44}$ (cgs units), valid for a Salpeter IMF. (*Right panel*) Mean dust attenuation in magnitudes as a function of redshift. Two versions of the attenuation factors are shown for UV-selected galaxies at $2 < z < 7$: one integrated over the observed population (open symbols), the other extrapolated down to $L_{FUV} = 0$ (filled symbols). Olive green dots data points are calculated by comparing the integrated FIR and FUV luminosity densities in redshift bins, rather than from the UV slopes or UV-optical SEDs.

measurements of the effective dust extinction, $\langle K_d \rangle$, as a function of redshift; this is the multiplicative factor needed to correct the observed FUV luminosity density to obtain the intrinsic value before extinction. The attenuation is usually estimated from the UV spectral slopes of star-forming galaxies using attenuation-reddening relations or occasionally from stellar population models fitting to the full UV-optical SEDs of galaxies integrated over the observed population. In estimating the SFH, each data-set has been corrected using the extinction factors relative to the corrispondent survey. Using this data, the resulting SFH (see Figure 3.3) fitting function is:

$$\psi(z) = 0.015 \frac{(1+z)^{2.7}}{1+[(1+z)/2.9]^{5.6}} \, M_\odot \, year^{-1} \, Mpc^{-3} \tag{3.3}$$

The emergent picture of the SFH is as follows: a rising phase, scaling as $\psi(z) \propto (1+z)^{2.9}$ at $3 \lesssim z \lesssim 8$, slowing and peaking at some point probably between $z = 2$ and 1.5, when the Universe was $\sim 3.5\, Gyr$ old, followed by a gradual decline to the present day, roughly as $\psi(z) \propto (1+z)^{2.7}$. The comoving SFRD at redshift 7 was approximately the same as that measured locally. The increase in $\psi(z)$ from $z \approx 8$ to 3 appears to have been steady, with no sharp drop at the highest redshifts.

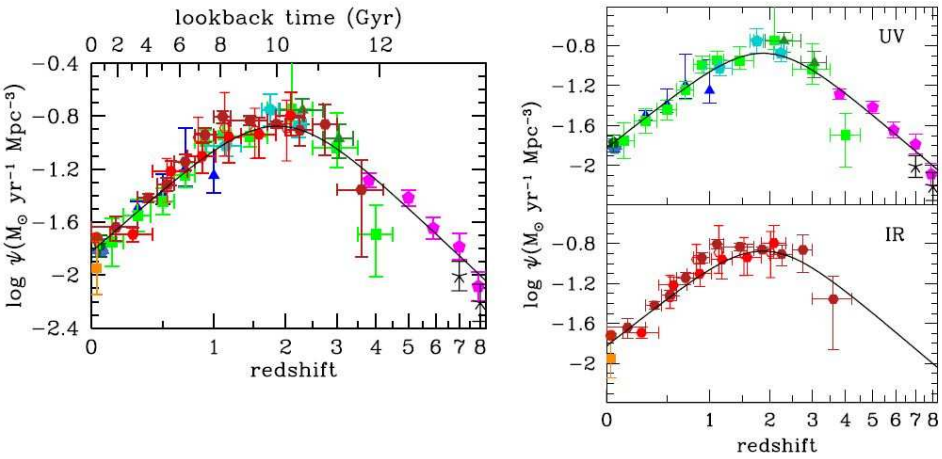

Figure 3.4 From Madau & Dickinson (2014): The history of cosmic star formation from (top right panel) FUV, (bottom right panel) IR, and (left panel) FUV+IR rest-frame measurements. The solid curve in the three panels plots the best-fit SFRD.

It is important to remark some important factors that can have an impact on this estimation:

- Each publication had a different approach to correct the data-sets for uncertainties in the derivation of the SFRD;
- Each study integrated their data to different luminosity limits, whereas in this estimate a fixed threshold of $0.03L^*$ is used;
- There are differences in the faint-end slopes for each data-set, which can yield large uncertainties in the relative integrated luminosity density.

3.2.1 A SFR problem: the comoving Stellar Mass Density

In their study, Madau & Dickinson (2014) proceed to do a comparison between the stellar formation history derived from the galaxy surveys and the comoving stellar mass density (SMD) from several other studies (see Figure 3.5).

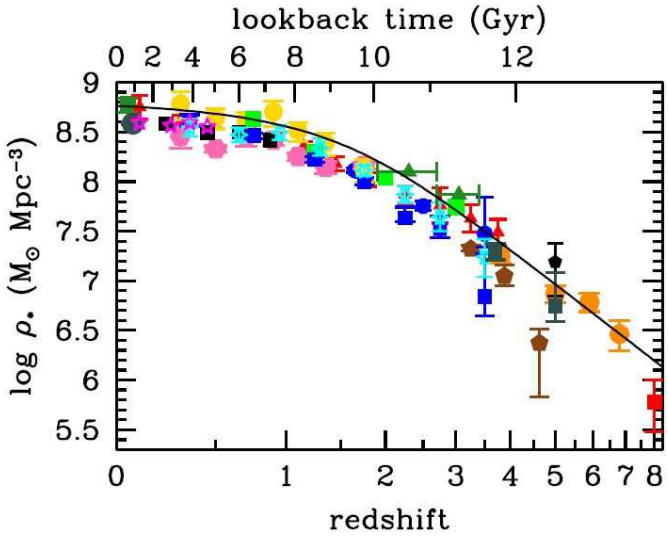

Figure 3.5 From Madau & Dickinson (2014): the evolution of the comoving stellar mass density. The solid line shows the global stellar mass density obtained by integrating the best-fit instantaneous star-formation rate density $\psi(z)$.

At high redshift, authors often extrapolate their stellar mass functions (SMFs) beyond the observed range by fitting a Schechter function. Stellar mass completeness is often not as well defined as luminosity completeness,

given the broad range of M/L values that galaxies can have. The model proposed by Madau & Dickinson (2014) appears to yield a systematically over-predicted comoving SMD in comparison with the literature, reaching an average excess factor of $\sim 60\%$ (see Figure 3.5), i.e. this model produces more low-mass stars than are actually observed, not contributing significantly to the total light of the galaxy. The author then proceeds to consider possible causes for this discrepancy:

- SFR could be overestimated, particularly at high redshift, when dust corrections for UVLF may be too large (even though the dust absorption is usually very severe); furthermore, there is the often-cited problem of probing the faint-end slope of both UVLF and IRLF;
- The comoving SMD could be underestimated: in fact, there is the problem of "outshining", where star-forming galaxies obscure older high M/L stars; there is literature suggesting that modeling stellar masses can lead to systematically underestimated stellar masses. That said, it is fair to remind that there can be factors working in the opposite direction (increasing the comoving SMD), like the effect of TP-AGB stars on NIR light, or a steeper low-mass slope to the SMF; at high redshift, most studies have found relatively flat low-mass SMF slopes, but galaxy samples may be incomplete for very faint, red, high-M/L galaxies;
- Strong nebular line emission can significantly affect broadband photometry for galaxies at high redshift, particularly at $z > 3.8$, where $H\alpha$ (and, at $z > 5.3$, [OIII]) enter the Spitzer IRAC bands;
- The problem could rely in the IMF: a more top-heavy or bottom-light IMF will lead to larger luminosities per unit SFR, hence smaller SFR/L conversion factors K; an IMF with a low-mass turnover will yield a larger mass return fraction R and proportionately lower final stellar masses for a given integrated past SFH.

3.2.2 A solution for the SFR problem

In an internal report, Franceschini et al. (2014) proposed a convincing explanation of this discrepancy through an analysis of far IR Herschel data, consisting in deep photometric imaging in six wavebands between 70 and $500\,\mu m$, that has made possible to better constrain the peak of dust emissions in the SEDs of active galaxies in order to estimate their bolometric IR emission (active galaxies include both star-forming and AGN-dominated ones). The study consists in statistical data from independent surveys (based on both Herschel and Spitzer data) through which robust bolometric LFs are calculated, essential to provide a reliable SFR estimate. Their model

considers four types of galaxy populations that make up the sample in order to effectively explain the number counts of the data taken into account:

- Normal spirals, that dominate the local source populations at $z < 1$ and become almost negligible at higher redshifts;
- Star-forming galaxies of moderate luminosities (LIRGs) that evolve fast in redshift up to $z \sim 1$, needed to explain the fainter number counts at all IR wavelengths; they are assumed to make up a $\sim 10\%$ fraction of the total galaxy population;
- Ultra-luminous infrared galaxies (ULIRGs) that dominate the IR emission from $z \simeq 1.5$, essential to explain the number counts at submillimeter and millimeter wavelengths; their typical luminosity appears to be $\sim 10^{11}\, L_\odot$ at $z \sim 1$ and $\sim 10^{12}\, L_\odot$ at $z > 1.5$. They are highly star-forming galaxies, with $SFR > 100\, M_\odot/year$. Spectral models for LIRGs and ULIRGS are very similar, the latter appearing to be broader with a significant enhancement at $\lambda \sim 60\, \mu m$ and in the submillimeter. The spectral shapes are well constrained by observational data;
- Type-I AGNs, that can easily be identified with combinations of optical IR colours; in the spectral model their SED is assumed a priori. Type-II AGNs, instead, are much more difficult to account for and the model does not try to identify them; instead, their contribution to the total IR emissivity is set up not to exceed a percentage of $\sim 30\%$, value that appears to be quite reliable based on previous literature.

These conditions fixed, the author then proceeds to make an estimate on SFR using the already known

$$SFR[M_\odot/yr] = KL_{bol}/L_\odot$$

thus assuming that the bolometric IR luminosity is a good tracer for star-formation, neglecting the contribution of low-mass long-lived stars, which is important only at $z \lesssim 0.4$. In order to obtain a complete sample for the SFR, the study must account for UV light not affected by dust absorption, adding GALEX surveys data (Arnouts et al. (2005)) and the VVDS data from Cucciati et al. (2012) in the analysis, thus providing a robust basis to construct a SFR model. For a further in-depth analysis, we refer to the original work. Figure 3.6 shows their results.

It is evident how their data show a systematic shift in SF activity towards lower redshifts compared to previous studies, in particular different from Madau & Dickinson (2014): their SFH has a peak at $z \simeq 2$, while Franceschini et al. (2014) found a peak value of $z \sim 0.8 - 1.2$ and then a

rather flat plateau at $z \sim 3$. Comparing both models to estimated fractional stellar mass in bins of stellar age by Gallazzi et al. (2008), it becomes evident that Franceschini et al. (2014) constructed a model that fits better the actual data: in fact, Gallazzi et al. (2008) found that 75% of the stellar mass is formed between 5.3 and 10.5 Gyrs of look-back time, better consistent with this model. The reason can be perhaps found in Madau & Dickinson (2014) overweighing the UV-selected data, which has far more uncertainties (due to dust absorption) than IR data. This problem can be solved through the analysis of the integrated comoving stellar mass density produced by star-forming galaxies, using the equation:

$$\rho_{star}(> z) = K \int_{z}^{z_{max}} dz' \rho_{IR+UV}(z') \left(\frac{dt}{dz'} \right) f_*[t(z) - t(z')] \tag{3.4}$$

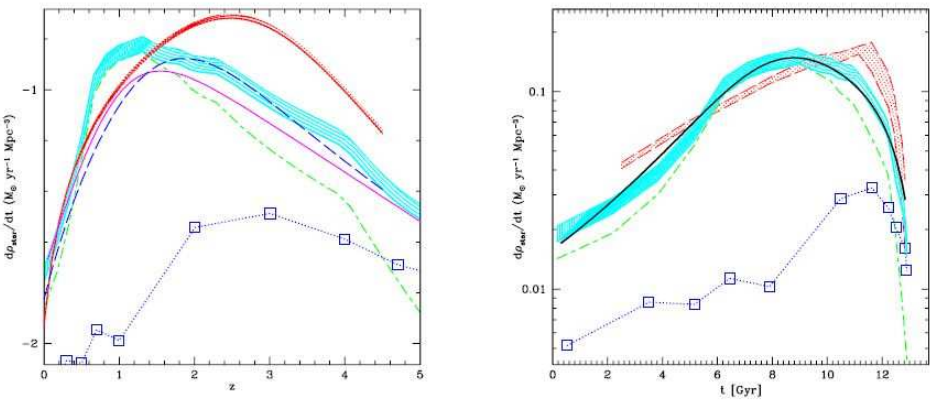

Figure 3.6 From Franceschini et al. (2014): (*Left panel*): the determined comoving star-formation rate density traced by IR and UV observations (cyan dotted strip, excluding type-I AGNs) compared with previous evaluations. The blue dashed curve is the best-fit from Madau & Dickinson (2014). The green long-short dash curve is the separate contribution to the SFR by IR-selected LIRGs and ULIRGs, the blue dotted line that derived from UV-selected samples without extinction corrections. All data are scaled to a Salpeter IMF. (*Right panel*): same as in the left, as a function of the cosmic look-back time. In the same panel the determined SF history is compared to model predictions based on the semi-analytic code by Ricciardelli and Franceschini (2010) (for a standard Salpeter IMF). The black continuous curve is an analytic fit to the presently determined total SFR density.

where f_* is the mass fraction of stars remaining at a certain epoch t after stars lose gas during evolution, putting it back into the ISM. Both this and the conversion factor K depends purely on the choice of IMF: the

conversion factor K for a standard Salpeter IMF $dn/dlogM \propto M^{-m}$ with $m = 1.35$ should be $K \simeq 1.63 * 10^{-10}$, whereas for a Chabrier IMF is $K \simeq 1.02 * 10^{-10}$, resulting in a 0.62 factor of conversion between the two models. The main difference between these two is that the Chabrier IMF converges to shallower slopes at masses lower than $1\,M_{\odot}$, while keeping the same slope at larger masses. As we shall shortly see, the latter yields a far better model for the comoving stellar mass density than the former does. Figure 3.7 shows that Franceschini et al. (2014) made a model that fits very well other independent determinations of the stellar mass density integrating the SFR with the choice of a Chabrier IMF, thus solving the discrepancy that the study by Madau & Dickinson (2014) first found.

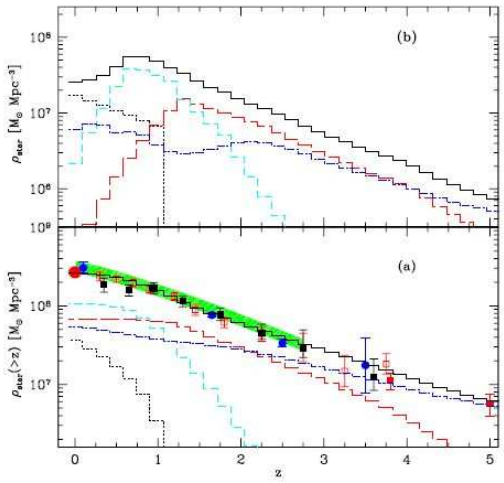

Figure 3.7 A comparison of published data on the comoving stellar mass-density in galaxies with predictions from Franceschini et al. (2014) based on Equation 3.4 and the assumption of a universal Chabrier IMF. Panel (a) reports the comoving integrated stellar mass-density (in $M_{\odot}/Mpc^3$) as a function of redshift obtained by integrating the SFR at all redshifts $> z$. Lines are: UV-selected SF (blue dot-dashed), ULIRGs (red long-dash), LIRGs (cyan short-dash), normal spirals (black dotted). All the data and the model curves have been rescaled to be consistent with a Chabrier IMF. Panel (b) shows the differential mass contributed by star-formation in redshift bins to the stellar mass-density in galaxies. Line types as in panel (a).

Chapter 4

The most recent developments: the radio

As it has been already mentioned in the Introduction, radio emission has recently raised astronomers' interest because of its independence from dust absorption and its fairly direct connection to star formation; this connection is regulated from the so-called IRRC (infrared-radio correlation), which we will examine in the respective section. The following section will present the main survey data studied in the literature which we will take into account for their SFR estimates; after that, we shall review such results and eventually examine the IRRC in a more deeply fashion.

4.1 Radio surveys: the COSMOS field

In the most recent years the developments in radioastronomy has obtained several deep surveys to investigate the Universe at high redshifts, radio emission being unaffected by dust absorption, thus providing an extraordinary observational tool to reach high distances and a clear view. One example is the work from Butler et al. (2017), who created a radio source catalogue in the $25\,deg^2$ XXL-South field by observing with the Australia Telescope Compact Array (ATCA) at 2.1 GHz. This catalogue focused its attention on AGNs, which are believed to contribute in galaxy evolution by feedback processes; in fact, studying the relative importance of star-forming galaxies and AGNs in the total radio emission at a given epoch is crucial to a better understanding of galaxy evolutionary models, in particular of the radio luminosity function (RLF). As already mentioned in the Introduction, high- and low-luminosity radio AGN form two distinct populations: the former show strong high-excitation emission lines and are subsequently called high-excitation radio galaxies (HERGs), the latter do not and their name is low-excitation radio galaxies (LERGs). It has been hypothesized that the difference between the two relies in different black hole accretion modes that

result in two distinct forms of feedback. To investigate these different types of populations, it is crucial to have tools like deep surveys over a relatively wide area; this also needs to be combined to reliable multiwavelength data to identify the optical/IR counterparts of radio sources, which are difficult to study alone due to their featureless radio spectrum. The ATCA radio observations in this field achieved a resolution of ~ 4.8" and are sensitive down to $\sigma \approx 41\,\mu Jy/beam$. This resulted in a catalogue of 6350 sources, 1677 of which were resolved, with a median spectral index of $\alpha = -0.75$. For a detailed description of the techniques and statistical tools used to bring up this result, we refer to Butler et al. (2017).

However, the main field which our review will focus on is the Cosmological Evolution Survey (COSMOS), a $2\,deg^2$ field observed with the most modern tools. These have provided a unprecedented amount of data with sensitivity and depth never reached before, thus opening a new window in cosmology. The COSMOS2015 catalogue by Laigle et al. (2016) contains $\sim 7.5 * 10^5$ objects for which precise photometric redshifts and stellar masses have been derived at NIR wavelengths; $\sim 6 * 10^5$ objects have been found in the $1.5deg^2$ UltraVISTA-DR2 region, and $\sim 1.5 * 10^5$ in the "ultra-deep stripes" ($0.62deg^2$) at $K_s \leq 24.7$, with the deepest regions reaching a 90% completeness limit of $10^{10}\,M_\odot$ to $z = 4$. NIR data catalogues are crucial to account for counterparts of radio sources and for accurate photometric redshifts and stellar mass estimates. This NIR-selected catalog uses WIRCam data covering the entire field, the UltraVISTA-DR2 data release, deep IR data from the *Spitzer* Larga Area Survey with Hyper-Supreme-Cam (SPLASH) project and optical data from the Hyper-Supreme-Cam. Furthermore, COSMOS2015 offers a match with X-ray, NUV, IR and FIR data from *Chandra*, GALEX, MIPS/*Spitzer*, PACS/*Herschel* and SPIRE/*Herschel*. This result is the first highly complete mass-selected samples to high and very high redshifts in an area of $54^2\,Mpc^2/h^2$ near $z \sim 1$. Again, for more technical details regarding the construction of the catalogue and the data analysis, see Laigle et al. (2016).

With respect to the radio survey, the largest and deepest one to date has been carried out by Smolčić et al. (2017b) with the VLA-COSMOS 3 GHz Large Project, made up from 384 hours of observations with the Karl G. Jansky Very Large Array (VLA) in S-band at 3GHz (10 cm) towards the already mentioned COSMOS field. This band was chosen for the observations for the combination of a large effective bandwidth ($\sim 2\,GHz$) and a fairly large field of view (half-power beam width 15') that allows to reach a high sensitivity, even though sources are typically fainter at this wavelength than they are at 1.4 GHz (the frequency of the very first COSMOS radio survey by Schinnerer et al. (2004)). It found 10830 radio sources down to 5σ, of which 67 are multi-component objects, reaching a median *rms* of $2.3\,\mu Jy/beam$ and an angular resolution of 0.75". Comparing their positions with those from the Very Long Baseline Array (VLBA)-COSMOS survey,

they computed an astrometry accuracy down to 0.01" at the bright end. The completeness of the sample has been estimated through Monte Carlo simulations. We refer to the original work for a more detailed view on the techinal characteristics.

The same authors then composed the most important catalogue for the purpose of studying the SFR: the multiwavelength one (Smolčić et al. (2017a)), with a particular focus on the faint radio population. They combined the data from the Smolčić et al. (2017b) catalogue with optical, near-infrared (UltraVISTA), mid-infrared (*Spitzer*/IRAC) and X-ray data (*Chandra*), finding counterparts for $\sim 93\%$ of the sources reaching out to $z \lesssim 6$. By matching data from the 3 GHz catalogue and from the 1.4 GHz one made possible to directly derive the spectral indices for 2530 sources; for the other ones, a spectral index of $\alpha = -0.7$ is assumed. The uncertainty on the spectral index can bring errors in the derived radio luminosity for a single object, uncertainties that however tend to be reduced on a statistical basis for an entire population. For NIR and MIR data, the already mentioned COSMOS2015 catalogue from Laigle et al. (2016) has been used, together with the i-band selected catalogue (see Scoville et al. (2007)) and the *Spitzer*-COSMOS InfraRed Array Camera 3.6 μm selected catalogue (IRAC); FIR photometry comes from the *Herschel Space observatory* observations in the COSMOS field.

The optical-MIR counterpart matching has been carried out through a nearest-neighbour criterion, accounting for a false match probability (p_{false}) for each match, based on Monte Carlo simulations, giving priority to COSMOS2015 counterparts, which are assigned if they are present within 0".8 and have $p_{false} \leq 20\%$. A total of 8035 counterparts is found. Concerning the redshift values, they are gathered from the available literature, giving priority to spectroscopic determinations over photometric ones; a total of 7778 redshifts out of the 8035 sources are retrieved. With these tools the authors then proceed to investigate the potential incompleteness of the COSMOS2015 catalogue, having cross-correlated radio and IR data: it is found that the incompleteness increases with the redshift, it being $\lesssim 1\%$ at $z < 2$ to $\sim 8\%$ at around $z \approx 5$. In order to study the star-formation history it is crucial to have a clean sample only made up of star-forming galaxies (SFG): so it is important to account for AGNs and exclude them. They have peculiar signatures in several aspects, so there are many ways to select them:

- Some AGNs have powerful X-ray emission, so the authors chose a X-ray luminosity limit of $L_X = 10^{42}\, erg\, s^{-1}$ above which a source is considered a X-ray AGN. They identify 859 AGNs in this way ($\sim 11\%$). Of course it cannot be excluded the presence of X-ray AGNs with a luminosity under this threshold;

- Another method to detect AGNs is the so-called MIR selection method,

that accounts for sources that contain a warm dusty torus consistent with the standard model for AGN. The presence of the torus gives a monotonic rise of flux in the four MIR bands which is easily identified; the authors found a total of 466 MIR AGNs, 229 of which had already been discovered through the X-ray criterion;

- SED-fitting analysis is another resource, a code based on a model that is used to disentangle the AGN contribution from the host-galaxy light. With this criterion 1178 AGNs are found, 669 of which were already identified through the first two methods. A total of 1623 AGNs are selected so far. AGN found with these three criteria are classified as moderate-to-high radiative luminosity AGN (HLAGN);

- In order to classify the remaining sample, a UV/optical color selection method is adopted. It separates sources based on the rest-frame NUV minus r^+-band colors corrected for dust extinction ($M_{NUV} - M_r$), identifying sources as *quiescent* if $(M_{NUV} - M_r) > 3.5$, of intermediate SF activity if $1.2 < (M_{NUV} - M_r) < 3.5$ or of high SF acticity if $(M_{NUV} - M_r 0 < 1.2)$. The latter are considered star-forming galaxies, while the former are thought to be red, quiescent, radio AGN host galaxies. From the remaining sample, 5410 are SFGs, 793 quiescent AGN host;

- Lastly, the authors investigate the excess of radio emission relative to star-formation rates. SFRs are obtained through SED-fitting of the total $(8 - 1000\,\mu m)$ infrared luminosity from the best-fit galaxy template, converted to SFR via the usual conversion factor scaled to a Chabrier IMF. Radio luminosity being an efficient SFR tracer, an excess in $log(L_{1.4GHz}/SFR_{IR})$ can arise from non-SFR processes, i.e. AGN-related. This function has a positive trend with redshift, so a redshift-dependent threshold is needed: $log(L_{1.4\,GHz}/SFR_{IR}) = 21.984(1 + z)^{0.013}$. Via this criterion, a total of 1846 radio-excess sources are found, part of which had already been identified through the other methods. Looking at Figure 4.1, it is evidente that a large fraction of the radio AGN hosted by red, quiescent galaxies shows an excess of radio emission, thus affirming their AGN nature. The $log(L_{1.4\,GHz}/SFR_{IR})$ distribution peaks close to that of SFGs, with a tail towards higher values, suggesting that a non-negligible amount of radio emission of these AGN comes from star-forming processes. AGN found with these three criteria are classified as low-to-moderate radiative luminosity AGN (MLAGN).

The final composition of the catalogue is as follows (see Figure 4.2):

- *Moderate-to-high radiative luminosity AGN (HLAGN)*, selected via X-ray, MIR color or SED-fitting methods. There has been found a total

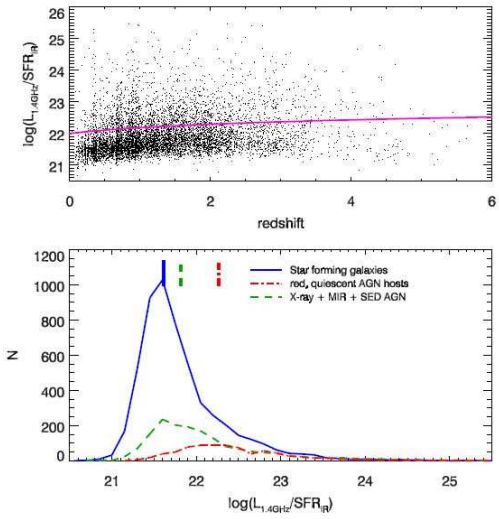

Figure 4.1 From Smolčić et al. (2017a). *Top panel*: ratio of rest-frame 1.4 GHz radio luminosity and infrared star-formation rate, $log(L_{1.4\,GHz}/SFR_{IR})$, as a function of redshift. The curve indicates the redshift-dependent threshold used to identify radio-excess sources. *Bottom*: distribution of $log(L_{1.4\,GHz}/SFR_{IR})$ for several (non-overlapping) galaxy populations as indicated in the panel.

of 1623 HLAGN in the 3 GHz sample of 7826 radio sources with associated IR counterparts, of which 486 ($\sim 30\%$) show a $> 3\sigma$ radio-excess in $log(L_{1.4\,GHz}/SFR_{IR})$. The fraction of HLAGN remains fairly constant in the range of $20 - 30\%$;

- *Star-forming galaxies (SFGs)* constitute what remains of the sample after removing HLAGNs and selecting galaxies with the dust-extinction corrected rest-frame color $(M_{NUV} - M_r) < 3.5$ or $(M_{NUV} - M_r) > 3.5$ if the source was also selected in the Herschel bands. A total of 5410 SFGs are identified, making up a $\sim 69\%$ of all the radio sources. The fraction of SFG increases from $\sim 10\%$ at $S_{3\,GHz} \sim 400 - 800\,\mu Jy$ to $\sim 60\%$ in the faintest flux bin at $S_{3\,GHz} \sim 50\,\mu Jy$;

- *Low-to-moderate radiative luminosity AGN (MLAGN)* are what remains of the sample, i.e. a total of 1648 sources. They are divided into two distinct sub-classes:

  - *Quiescent-MLAGN* are selected from a $(M_{NUV} - M_r) > 3.5$ criterion for a total of 793 sources. The fraction of MLAGN decreases from $\sim 75\%$ at $S_{3\,GHz} \sim 400 - 800\,\mu Jy$ down to $\sim 50\%$ at $S_{3\,GHz} \sim 100 - 400\,\mu Jy$, and further to $\sim 20\%$ at $S_{3\,GHz} \sim 50\,\mu Jy$;

  - *Radio-excess-MLAGN* are selected objects with a $> 3\sigma$ radio-

excess in the $log(L_{1.4\,GHz}/SFR_{IR})$ redshift-dependent distribution for a total of 1360 sources, 505 of which overlap with the quiescent-MLAGN sample and 855 with the SFGs sample.

It is evident that the combined AGN sample (HLAGN and MLAGN) dominates the radio population at $S_{3\,GHz} > 100\,\mu Jy$, while at the faintest end at $S_{3\,GHz} \sim 50\,\mu Jy$ the bulk of the population is constituted by SFGs ($\sim 60\%$). Focusing on the bottom panel, where data concercing radio-excess features are plotted, it is evident that the fraction of sources with total radio luminosity consistent with that expected from star-formation increases with decreasing flux density from $\sim 10\%$ at $S_{1.4\,GHz} \sim 700 - 1000\,\mu Jy$ to $\sim 75\%$ at $S_{1.4\,GHz} \sim 50\,\mu Jy$, while it decreases for sources with radio-excess from $\sim 90\%$ to $\sim 15\%$. The switch between the two dominating populations happens at $S_{1.4\,GHz} \sim 200\,\mu Jy$.

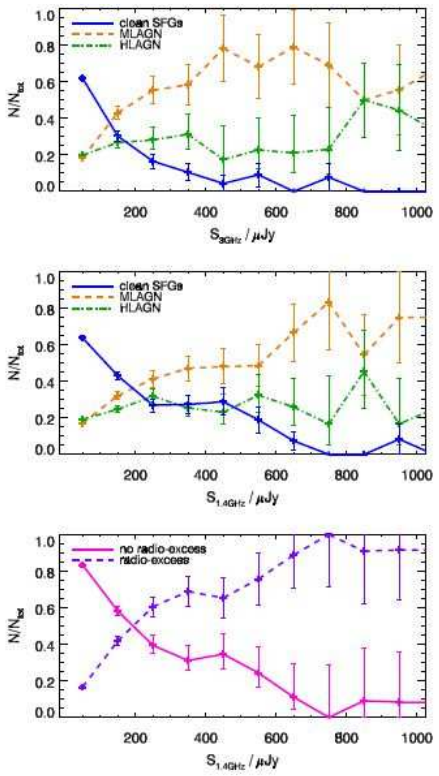

Figure 4.2 From Smolčić et al. (2017a). Fractional contributions of the various populations (indicated in the panels) as a function of 3 GHz flux (top panel), and 1.4 GHz flux (middle and bottom panels).

4.2 SFR estimates through radio data

One of the first attempts to derive SFRs from the COSMOS data was made by Smolčić et al. (2009), using a sample of 340 SF galaxies with $z \leq 1.3$ selected via a rest-frame optical-color-based method. Even though several other studies have focused their attention on SFR from surveys with radio data, we will refer only to the most recent and reliable one from Novak et al. (2017), based on the VLA-COSMOS 3GHz Large Project, thoroughly reviewed in the previous section. Their results will be compared with those from previous literature, including Smolčić et al. (2009). In this study, SFRs are scaled to a Chabrier IMF, that we found to be the best choice for the initial mass function in Chapter 3. As the purpose of their work is estimating star-formation whether the galaxy is an AGN-host or not, it is not necessary to discard all AGN-hosts from the sample, but they limit themselves to remove all sources dominated by AGN radio emission. This task is achieved through the already mentioned radio-excess method, with a dependence on the redshift quantified as:

$$r = log\left(\frac{L_{1.4\,GHz}[W\,Hz^{-1}]}{SFR_{IR}[M_{\odot}\,yr^{-1}]}\right) > 22 * (1+z)^{0.013} \tag{4.1}$$

This criterion yields a total of 1814 (23%) sources dominated by AGN emission, making the final sample constituted by 5915 SFGs (it is important to say, however, that the estimate of the SFRD has been also calculated on a free-AGN sample, yielding a result with a decrease of 0.035 dex, value that is within the uncertainties of the final result). Assuming the radio spectrum described as a simple power law $S_{\nu} \propto \nu^{\alpha}$, the consequent K-correction results $K(z) = (1+z)^{-(1+\alpha)}$. Usually, this correction factor yields the largest uncertainties on the results. The authors tested its influence by repeating the final SFRD estimate with values of $\alpha = -0.7$ and $\alpha = -0.8$, finding results within the uncertainties of the nominal sample. So, the results that will be obtained can be considered robust. The final expression for the rest-frame luminosity is therefore:

$$L_{\nu_1} = \frac{4\pi D_L^2(z)}{(1+z)^{1+\alpha}}\left(\frac{\nu_1}{\nu_2}\right)^{\alpha} S_{\nu_2} \tag{4.2}$$

where S_{ν} is the monochromatic flux density at two frequencies, α is the spectral index, L_{ν} is the rest-frame luminosity and D_L is the luminosity distance. As assessed in the previous section, the spectral index is directly derived if the comparison between 1.4GHz and 3GHz observations is available, otherwhise a common value of $\alpha = -0.7$ is assumed. To compute the LF $\Phi(L, z)$, the density of sources is needed; in fact the LF gives the number

of radio sources in a comoving volume per logarithm of luminosity:

$$\Phi(L,z) = \frac{1}{\Delta logL} \sum_{i=1}^{N} \frac{1}{V_{max,i}} \tag{4.3}$$

where $V_{max,i}$ is the maximum observable volume of the i-th source, $\Delta logL$ is the width of the luminosity bin and the sum goes over each source i in a given redshift and luminosity bin. To account for any effects that can lead to an incompleteness of the sample, the most general expression to calculate the V_{max} is:

$$V_{max,i} = \sum_{z=z_{min}}^{z_{max}} [V(z+\Delta z) - V(z)]C(z) \tag{4.4}$$

where $C(z)$ is a redshift-dependent geometrical and statistical correction factor that takes the observed area and sensitivity limit into account (see Novak et al. (2017) for more details). The completeness limit of the catalogue is that described in Smolčić et al. (2017a). Radio LF are usually parametrized as follows:

$$\Phi_0(L) = \Phi_* \left(\frac{L}{L_*}\right)^{1-\alpha} exp\left[-\frac{1}{2\sigma^2} log^2\left(1+\frac{L}{L_*}\right)\right] \tag{4.5}$$

where the L_* parameter describes the position of the turnover of the distribution, Φ_* gives the normalization, α and σ respectively fit the faint and bright end of the distribution. This survey well costrains the bright end of the LF, but the faint one needs extrapolation from data of wide surveys. Parameters' values that best achieve this task are: $\Phi_* = 3.55 * 10^{-3}\, Mpc^{-3}\, dex^{-1}$, $L_* = 1.85 * 10^{21}\, W\, Hz^{-1}$, $\alpha = 1.22$ and $\sigma = 0.63$. Assuming that the shape of the LF does not change overtime, the authors allow only pure luminosity evolution (horizontal shift in the $logL - log\Phi$ plane) or pure density evolution (vertical shift), which are parametrized as:

$$\Phi(L,z,\alpha_D,\alpha_L) = (1+z)^{\alpha_D} \Phi_0 \left(\frac{L}{(1+z)^{\alpha_L}}\right) \tag{4.6}$$

where α_D represents pure density evolution and α_L the pure luminosity one. In order to create a single model for the evolution of star-forming LF, the authors fit all LF points in all redshift bins with a two-parameters pure luminosity evolution (a pure density one would bring a much higher SFRD estimate in comparison to current literature, but this is indeed a simplification):

$$\Phi(L,z,\alpha_L,\beta_L) = \Phi_0 \left[\frac{L}{(1+z^{\alpha_L+z\beta_l})}\right] \tag{4.7}$$

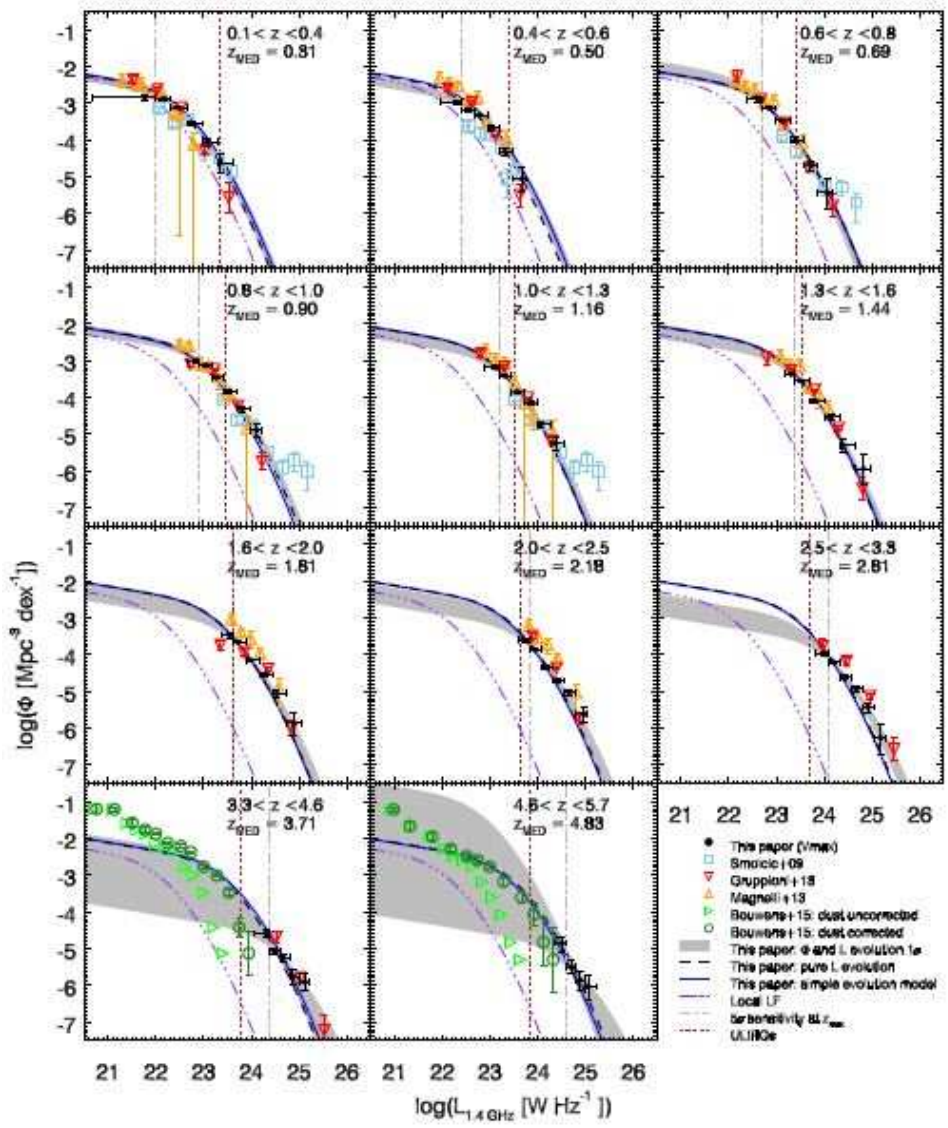

Figure 4.3 From Novak et al. (2017). Radio luminosity functions of star-forming galaxies in different redshift bins (black filled circles). Best-fit pure luminosity evolved function in each redshift bin is shown with black dashed lines. Combined luminosity and density evolution are shown in the gray shaded area. The local radio function is shown for reference as a triple-dot-dashed purple line. The vertical dot-dashed line corresponds to the 5σ luminosity limit at the high redshift end of the bin ($1\sigma = 2.3\,\mu Jy\,beam^{-1}$ at 3 GHz). The vertical red dotted line at the center of each panel defines the radio luminosity corresponding to ULIRGs under the assumption of redshift evolving q_{TIR}. All data shown for comparison are indicated in the bottom right corner, among which Gruppioni et al. (2013) and Smolčić et al. (2009) can be found.

Estimate of the parameters are $\alpha_L = 3.16 \pm 0.2$ and $\beta_L = -0.32 \pm 0.07$. All results are visible in Figure 4.3.

In order to estimate the SFR from radio data, the authors use the so-called IR-radio correlation (IRRC), which will be further analyzed in the following section. This link is regulated by the q_{TIR} parameter:

$$q_{TIR} = log\left(\frac{L_{TIR}}{3.75 * 10^{12}\, W}\right) - log\left(\frac{L_{1.4GHz}}{W\, Hz^{-1}}\right) \tag{4.8}$$

As we shall see, Delhaize et al. (2017b) found a slight evolution of the q_{TIR} parameter with redshift, parametrized as follows:

$$q_{TIR}(z) = (2.78 \pm 0.02) * (1+z)^{-0.14 \pm 0.01} \tag{4.9}$$

The final expression that converts radio luminosity into SFR is:

$$\frac{SFR}{M_\odot\, yr^{-1}} = f_{IMF} * 10^{-2} * 10^{q_{TIR}} \frac{L_{1.4\,GHz}}{W\, Hz^{-1}} \tag{4.10}$$

where $f_{IMF} = 1$ for a Chabrier IMF. After that, the star-formation rate density SFRD of a given epoch is obtained through an integral:

$$SFRD = \int_{L_{min}}^{L_{max}} \Phi(L, z, \alpha_D, \alpha_L) * SFR(L) dlogL \tag{4.11}$$

Results are shown in Figure 4.4, for several luminosity ranges:

- *Entire luminosity range*: this means setting $L_{min} = 0$ and $L_{max} \longrightarrow +\infty$. It is visible how the major contribution to the SFRD comes from galaxies with luminosity around the turnover of the LF. Unfortunately, at high redshift the faint end of the LF is only extrapolated, so this cannot be considered a reliable estimate;

- *Data constrained limits*: L_{min} and L_{max} are set, respectively, to be the lowest and highest value of the observed luminosty function;

- *ULIRGs*, i.e. galaxies with IR luminosity of $10^{12}\, L_\odot < L_{TIR} < 10^{13}\, L_\odot$. This kind of galaxies forms stars very efficiently, with $SFR \sim 100 - 1000\, M_\odot\, yr^{-1}$, and they are very well constrained by the survey data under exam;

- *HyLIRGs*, i.e. galaxies with IR luminosity of $L_{TIR} > 10^{13}\, L_\odot$, with extreme star-formation activity ($SFR > 1000\, M_\odot\, yr^{-1}$).

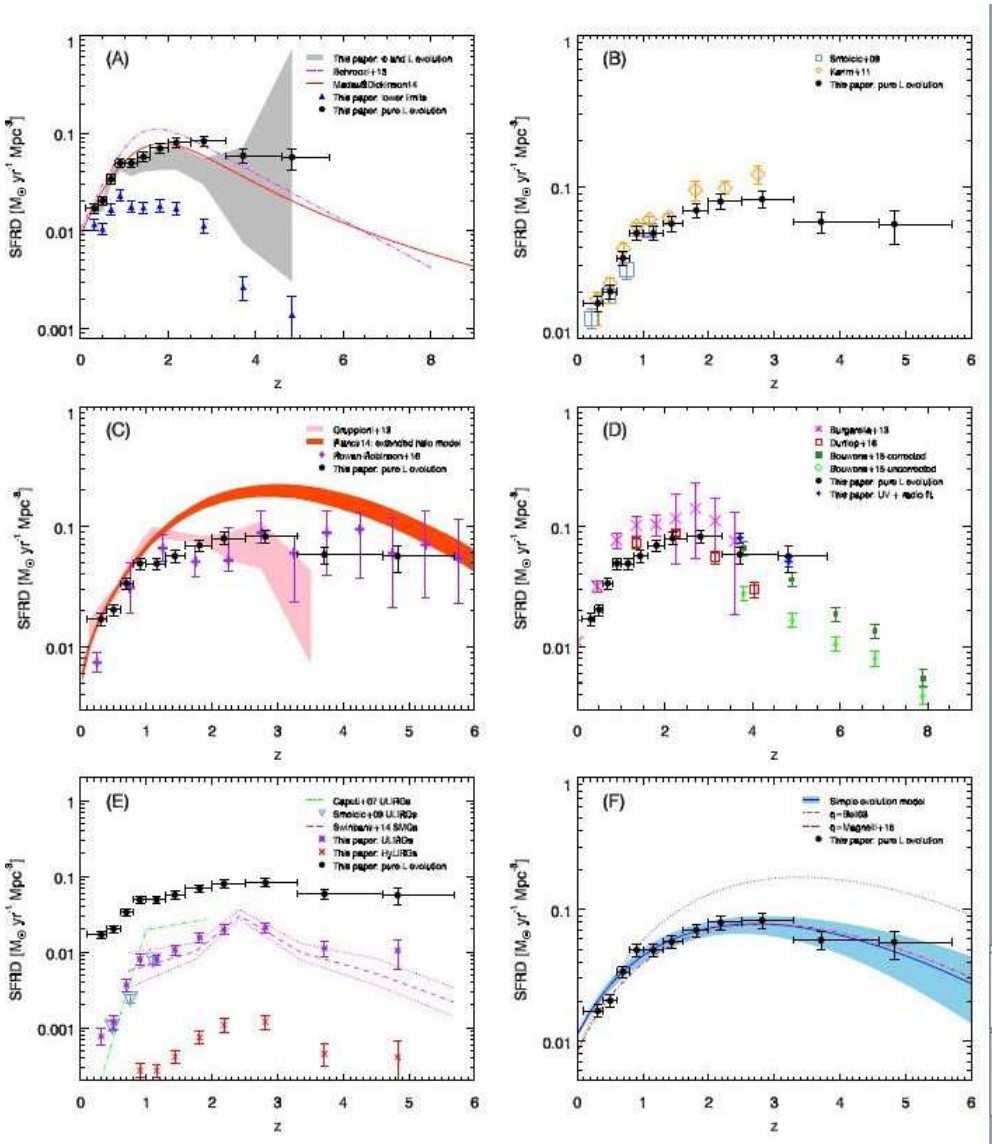

Figure 4.4 From Novak et al. (2017). Cosmic star formation rate density (SFRD) history. The total SFRD values estimated from the pure luminosity evolution in separate redshift bins are shown as filled black circles in all panels. All data shown for comparison are indicated in the legend of each panel.

4.3 The IR-Radio correlation (IRRC)

Delhaize et al. (2017b) examined, in their work, the behaviour of the IRRC over the range $0 < z \lesssim 6$ using the same data that we already saw (3GHz observations with the VLA plus IR data from Herschel, both in the COSMOS field), applying their analysis on a resulting clean sample constituted by 9575 sources, without AGNs whatsoever, removed via the method already seen in Smolčić et al. (2017a).

The IRRC is based on the 1.4GHz luminosity, but the original sample is made through observations at 3GHz; so, a conversion is necessary, from the 3GHx fluxes into 1.4Hz luminosities:

$$L_{1.4\,GHz} = \frac{4\pi D_L^2}{(1+z)^{\alpha+1}} \left(\frac{1.4}{3}\right)^{\alpha} S_{3\,GHz} \tag{4.12}$$

Concerning the total IR luminosities (L_{TIR}), they are derived by integrating the best-fitting galaxy template to the SED between $8 - 1000\,\mu m$ in the rest-frame. As we already saw the IRRC is parametrized as follows:

$$q_{TIR} = log\left(\frac{L_{TIR}}{3.75 * 10^{12}\,Hz}\right) - log\left(\frac{L_{1.4\,GHz}}{W\,Hz^{-1}}\right) \tag{4.13}$$

The results are plotted in Figure 4.5.

As one can easily see, there is a slight but non-neglectable decrease of q_{TIR} with redshift. The authors proceed to account for possible bias in their data. The first hypothesis is whether upper and lower limits have a deep impact on the data: the answer is yes, in fact the median value of q_{TIR} derived ignoring the limits has a flatter fit, but the decreasing trend does not disappear. Then they account for the presence of any misclassified HLAGN that could be contaminating the sample via X-ray stacking, but the analysis does not indicate a strong presence of remaining AGNs; even if this result was not correct, deriving the q_{TIR} for the non-clean sample brings only a modest decrease in the normalisation of the fit, indicating that the potential presence of HLAGN would not dramatically influence the results. Instead, a massive presence of non-detected radio-excess objects could have a non-negligible influence, as found via a similar analysis.

Another factor that influences deeply the q_{TIR} is the choice of the spectral index, i.e. the K-corrections. In fact, estimating the difference in q_{TIR} with two of the most accredited value for the spectral index ($\alpha_1 = -0.7$ and $\alpha_2 = -0.8$), the authors find:

$$\Delta q_{TIR}(\alpha_1, \alpha_2) = -0.1 log(1+z) + 0.033$$

Decreasing the spectral index systematically lowers the q_{TIR} and steepens the (1+z) dependence. Other possible culprits for this trend could be

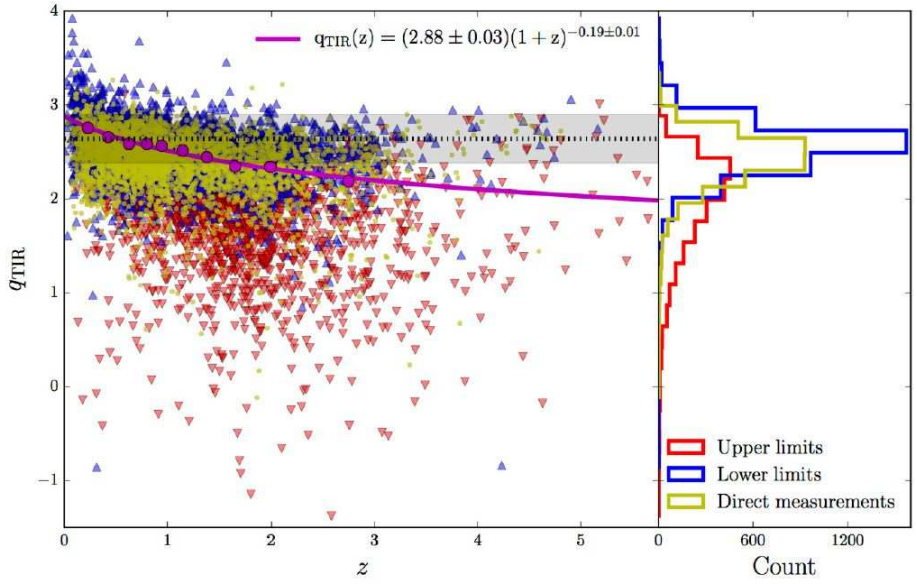

Figure 4.5 From Delhaize et al. (2017b). IRRC (q_{TIR}) versus redshift for star-forming galaxies. Objects with detections in both the infrared and radio have directly-constrained values of q_{TIR} and are shown as yellow points. Objects only detected in the radio are upper limits and shown as red triangles. Objects only detected in the infrared are lower limits and shown as blue triangles. A doubly-censored survival analysis has been used to calculate the median q_{TIR} within redshift bins, indicated by the magenta points. Error bars represent the 1σ dispersion calculated via the bootstrap method. The magenta line shows the power-law fit to these. In the right-hand panel, the q_{TIR} distribution is shown separately for direct measurements, upper limits and lower limits.

the uncertainties in the K-corrections or other physical factors like an increasing magnetic field strength or major mergers of galaxies, although these hypothesis are not easily verifiable.
So, under the assumptions of linear IRRC, power-law radio spectrum and IR emission constituing a good tracer for SFR, one can use this correlation to derive SFR from radio emission. The final results are:

$$q_{TIR}(z) = (2.88 \pm 0.03)(1+z)^{-0.19\pm0.01}$$
$$q_{TIR}(z) = (2.85 \pm 0.03)(1+z)^{-0.22\pm0.01}$$

for $\langle\alpha\rangle = -0.7$ and $\langle\alpha\rangle = -0.8$, respectively.

Chapter 5

Submillimetric observations

MIR and FIR observations require space-based telescopes, but at submillimeter and millimeter wavelengths observations can be made from the ground within certain atmospheric transmission windows. The advent of submillimeter bolometer array cameras such as SCUBA on the JCMT was a revolution in the field, opening a new window for cosmology studies, for example leading to the first detections of a large population of ULIRGs at high redshift, a thousand times more abundant in the early Universe than at the present day. Dust continuum emission in the submillimeter range is one of the most reliable tracers of the earliest phases of star-formation since it directly probes the dense interstellar material from which the stars form: since dust emission in the submm is optically thin, it is directly proportional to the mass of material (assuming a constant temperature) and leads to the detection of all proto-stellar objects or pre-stellar clumps and cores.

Until recently, only the most luminous high-z objects could be detected, but the new ALMA interferometer improved detection sensitivities by more than an order of magnitude, even though over small fields of view. Submillimeter observations have the credits of measuring emission beyond the peak of dust emission, where flux is declining steeply with wavelength in the Rayleigh-Jeans part of the SED. This leads to a negative K-correction so strong that it blanks out the effects of distance: a galaxy with a given IR luminosity will have roughly constant submillimeter flux if it is observed at any redshift $1 < z < 10$. By contrast, the bolometric corrections from the observed submillimeter wavelengths to the total IR luminosities are large and depend strongly on dust temperature. This can lead to significant uncertainties in interpreting submillimeter fluxes from high-redshift sources, and a bias towards detecting galaxies with the coldest dust emission. So, these are the main reasons why this galaxy population cannot be efficiently observed at radio wavelengths: first, the radio-identified SMGs are mostly bright in the submillimeter, so their properties may not be representative. Second, the radio flux drops at high redshifts due to the positive K-correction of

the radio synchrotron emission, while the submillimeter flux remains almost invariant. Compton cooling on the cosmic microwave background (CMB) radiation may also significantly reduce the 20 cm emission in the highest redshift sources. Thus, the radio identification technique is biased against high-redshift sources. Finally, many SMGs have been found to have more than one candidate radio counterpart, making identifying the correct counterpart to the SMG difficult.

So, submillimeter observations cover a crucial role in observing dusty star-forming galaxies at high redshift, because they allow to account for star-formation activity that would not be otherwhise detected. In practice, the greatest limitation for deriving LFs or SFRD is identifying galaxy counterparts to submillimeter sources and measuring their redshifts. This limitation is due mainly to the large beam-size of single-dish submillimeter observations (limitation that is overcome with ALMA, it being an array of radiotelescopes), but it is also due to the fact that the optical counterparts are often very faint and sometimes invisible. Another consequence of the negative K-correction is that substantial redshift uncertainties translate to only relatively small uncertainties in the bolometric luminosity. Hence, using radio-identified counterparts and very rough radiomillimetric redshift estimates, one is able to make plausible estimates of the SFRD from submillimeter sources in broad redshift bins. Many analyses demonstrated a significant contribution of dusty submillimeter galaxies (SMGs) to the cosmic SFRD at high redshift with SFR values of $\sim 100\, M_{\odot}\, year^{-1}$, mainly limited to $z \lesssim 4$, but recent discoveries have pointed out their substantial presence out to $z = 6.3$; it is thought that SMGs are the progenitors of massive elliptical galaxies in the local Universe.

We shall now present a brief review of the evolution of this rather new field, focusing our attention on the most important results that shall suit better our purposes.

5.1 Historical data

The Submillimeter Common-User Bolometer Array (SCUBA) on the James Clerk Maxwell Telescope (JCMT) was one of the first tools that allowed the discovery of the SMGs population in the 90's. Several surveys have been carried out since then with this instrument, we shall now review a number of them.

One of the first and most important work was from Chapman et al. (2005), who used a sample of SMGs of 150 sources detected at $850\,\mu m$ ($> 3\sigma$), combining these objects with their available radio counterpart (for 98 of them, from the 1.4GHz VLA radio survey) to derive robust redshift estimates, crucial basis for a good analysis. The redshift distribution of the data displays a marked peak at $z \sim 2.0 - 2.5$. In order to conduct a SFR

analysis, the authors needs to account for AGN presence; from the 98 radio-SMG for which spectroscopic observations are available: 18% show obvious AGN characteristics; 31% are apparently star-forming galaxies; 25% are difficult to classify, but remain reasonable candidates to be star-forming galaxies; and 26% are spectroscopically unidentified, and so are unlikely to be strong AGN at $z < 1.2$ or $z > 1.8$ (but could be star-forming galaxies with weak/absent emission lines at almost any redshift). After deriving the bolometric IR luminosity with the usual IRRC (a constant one, at the time), the authors try to see whether the recipe for deriving SFRs for UV-selected galaxies works on this rest-frame FIR-selected population or not. They find a deep discrepancy (of a 100 factor) between UV- and radio-inferred SFR, probably because of a deep bias against dust obscuration in the UV wavelengths. Following the same procedure seen multiple times by now and after assessing a star-forming objects dominated sample with an estimated maximal contribution by AGN activity of 30% (see Chapman et al. (2005) for further details), their derived SFRD is portrayed in Figure 5.1, with a fit of $SFRD = 1.26 * exp[-(z - 2.18)^2/\sigma^2]$ with $\sigma = 1.30$.

One important thing to notice is the relative evolution of the UV- and submm-selected populations: in fact SMGs are coeval and energetically comparable in a volume-average sense with the population of UV-bright, star-forming galaxies detected at $z \sim 2 - 3$. However, the SMGs with $S_{850\,\mu m} > 5\,mJy$ and UV-selected galaxies clearly do not evolve in the same manner. SMGs appear to evolve more strongly than the UV-selected population out to $z \sim 2$ and seem to behave in a manner very similar to luminous Quasars and X-ray selected AGN, whose luminosity density peaks at $z \sim 2.3$. As Figure 5.1 makes clear, this is in stark contrast with the individually-less luminous, UV-selected galaxies whose comoving luminosity density is approximately constant out to at least $z \sim 5$. This suggests that the properties of the bright submm population is more closely linked with the formation and evolution of the galaxies or galactic halos which host QSOs, than the more typical, modestly star-forming galaxies identified from their rest-frame UV emission. The SMGs appear to be prodigiously forming stars, with the modest X-ray luminosities of SMGs suggesting either low rates of accretion onto super-massive black holes (SMBHs) and/or moderate SMBH masses. The authors conclude that the SMGs are indeed an early phase in the evolution of a massive galaxy, forming many stars quickly over $\sim 10\,kpc$ spatial scales, as shown by the extended radio emission tracing UV structures. As the merger proceeds, the growing SMBH will begin to accrete material more quickly as instabilities drive material to more concentrated configurations. The SMBH thus grows even more rapidly, on a timescale which is delayed from that of the initial starburst, eventually blowing channels through the dust and becoming visible as a QSO. Of course, this is only a possible explanation, and the relationship between SMGs and other galaxy populations probably spans a range of scenarios and evolutionary

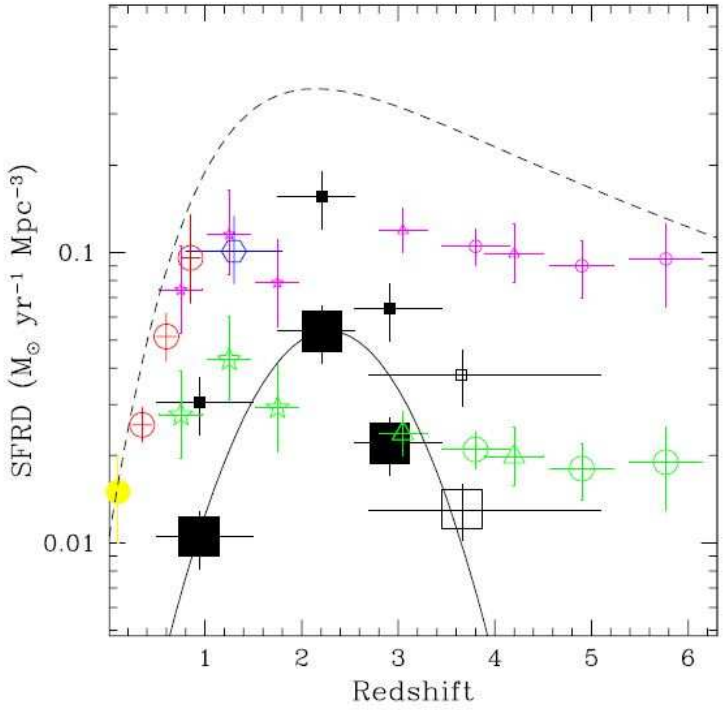

Figure 5.1 The evolution of the energy density (parametrized by SFRD) in the Universe with epoch. Chapman et al. (2005) measurements (large squares, shown at the median value for each redshift bin) are compared to the published estimates from optical/UV surveys and radio/IR tracers of the star formation density. The open square indicates the SMGs without radio identification. The smaller symbols for the optical estimates indicate dust-corrected estimates. A Gaussian fit is shown for the four submm galaxy points, tracing an evolution comparable to luminous radio-selected Quasars. For the submm sources, the smaller points show a simple redshift-independent correction to the luminosity density to match the submm extragalactic background down to 1 mJy. The dashed line is the best fit for a simple parametric model constrained by the counts of sources in the FIR/submm.

histories, and more comprehensive models are required to understand and further test the evolution of SMGs. A step forward in this direction was made by Tacconi et al. (2008), who made sub-arcsecond resolution IRAM PdBI millimeter CO interferometry of four $z \sim 2$ SMGs extracted from the same data as Chapman et al. (2005) with the hypothesis of a Chabrier IMF. This data revealed for the first time spatially resolved CO gas kinematics in the observed SMGs, with results suggesting that the star-forming gas is in compact, rotating disks. This brought compelling evidence that these SMGs represent extreme, short-lived maximum star-forming events in highly dissipative mergers of gas rich ($> 30\%$ gas fraction) galaxies. From the ratio of the comoving volume densities of SMGs and quiescent galaxies in the same mass and redshift ranges, and from the comparison of gas exhaustion time scales and stellar ages, they estimated a SMG phase duration of about 100 Myrs via two ways: from the ratio of the cosmic volume density of SMGs and that of the quiescent population in the same mass and redshift ranges, as the latter are plausibly the descendants of the former, and from the comparison of stellar ages and gas exhaustion time scales, obtaining comparable results.

One of the first surveys carried out by SCUBA was the SCUBA Half-Degree Extragalactic Survey (SHADES), conducted in 2003-2005. The SHADES survey was conducted in two fields, each with abundant multi-wavelength supporting survey data. The $\sim 0.1\,deg^2$ surveyed by SHADES in the Lockman Hole East field, in particular, has some of the best Spitzer Space Telescope data. The obtained results are presented in a series of papers. Paper I presented the survey design, motivation and data analysis. Paper II (Coppin et al. (2006)) presented further data analysis, the source counts, the catalogues and the maps. In Paper III, Ivison et al. (2007) carried out the radio and/or MIR counterpart catalogue using 1.4-GHz radio imaging from the National Radio Astronomy Observatorys (NRAO) Very Large Array (VLA) and $24\,\mu m$ data from Spitzer. This data-matching allows for precise astrometric measurement of submm data thus enabling robust spectroscopic investigations. The authors identified solid counterparts to over two thirds of the sample (54 and 46 per cent at 1.4GHz and $24\,\mu m$, respectively), presenting optical, $24\,\mu m$ and radio images of each SMG, also finding a median redshift of 2.8 for the radio-identified sample; many more follows, but we do not review them all here.

Another important instrument created for submillimeter astronomy was the Atacama Pathfinder Experiment (APEX), located in a 5100m high site in Chajnantor, specifically modeled to observe the dusty regions of the inner Milky Way (Schuller et al. (2009)). The Large APEX Bolometer Camera (LABOCA) is a 295-element bolometer array observing at $870\,\mu m$, with a beam size of 19.”2. Taking advantage of its large field of view (11.′4) and sensitivity, the first unbiased survey of the entire Galactic Plane was created, with a typical noise level of $5070\,mJy/beam$: the APEX Telescope Large

Area Survey of the Galaxy (ATLASGAL). They first covered $\sim 95\,deg^2$ of the Galactic Plane. These data revealed ~ 6000 compact sources brighter than 0.25 Jy (63 sources per square degree), as well as extended structures, many of them filamentary. About two thirds of the compact sources have no bright infrared counterpart, and some of them are likely to correspond to the precursors of (high-mass) proto-stars or proto-clusters. With a 5σ detection limit of $250\,mJy/beam$, this survey is complete for proto-stellar cores down to $\sim 10\,M_\odot$ at 2 kpc, or $\sim 50\,M_\odot$ at 5 kpc.

Apart from that, many other surveys have been carried out with the LABOCA camera; one example is the LABOCA Extended Chandra Deep Field South (ECDFS) Submillimetre Survey (LESS). LESS mapped the full 300x300 ECDFS at $870\,\mu m$ to a noise level of $\sigma_{870\,\mu m} \approx 1.2\,mJy\,beam^{-1}$, for a beam with angular resolution of 19."2. 126 SMGs were detected at $> 3.7\sigma$ significance (equivalent to a false-detection rate of $\sim 4\%$). Wardlow et al. (2011) used this data to derive redshifts and other physical properties of the sample, like the inferred SFRD. The derived photometric redshift distribution peaks at $z = 2.2 \pm 0.1$. Comparing this value to the photometric redshift distribution of SMG counterparts in the SHADES survey and to the spectroscopic sample from Chapman et al. (2005), the authors found a consistent result with the latter, both being peaked at higher redshifts than the SHADES SMGs. This survey is more complete and with a deeper sample than the SHADES one, so this discrepancy is accountable to a lack of data of the latter. The redshift distribution value now assessed is based only on submillimeter data with radio and/or IR counterparts; to account for any possible bias, the authors employ a statistical analysis in order to estimate the redshift distribution for the entire sample. They statistically identified the redshifts of $\sim 60\%$ of the unidentified SMGs, and showed that the remainder likely lie at $z \gtrsim 3$: their most likely median redshift for the $S_{870\,\mu m} \gtrsim 4\,mJy$ SMG population is $z = 2.5 \pm 0.6$. The submillimetre-to-radio flux ratio in SMGs is mainly influenced by redshift and the characteristic dust temperature. Chapman et al. (2005) assumed a dust emissivity, $\beta = 1.5$, and the $z = 0$ far-infrared-radio correlation, to determine empirically the dust temperature for their sample of SMGs:

$$T_D = \frac{6.25(1+z)}{(S_{850\,\mu m}/S_{1.4\,GHz})^{0.26}} \tag{5.1}$$

Then, assuming a constant IRRC for a spectral index $\alpha = 0.8$ ($q_{FIR} = 2.64$) to calculate far-infrared luminosities of the LESS SMGs from their radio fluxes, as done by Chapman et al. (2005), and employing the V_{max} method for deriving luminosity densities, they derived the SFRD (Figure 5.2).

A percentage up to 45% of the LESS SMGs do not have robustly identified optical counterparts, so they accounted for this population by assigning

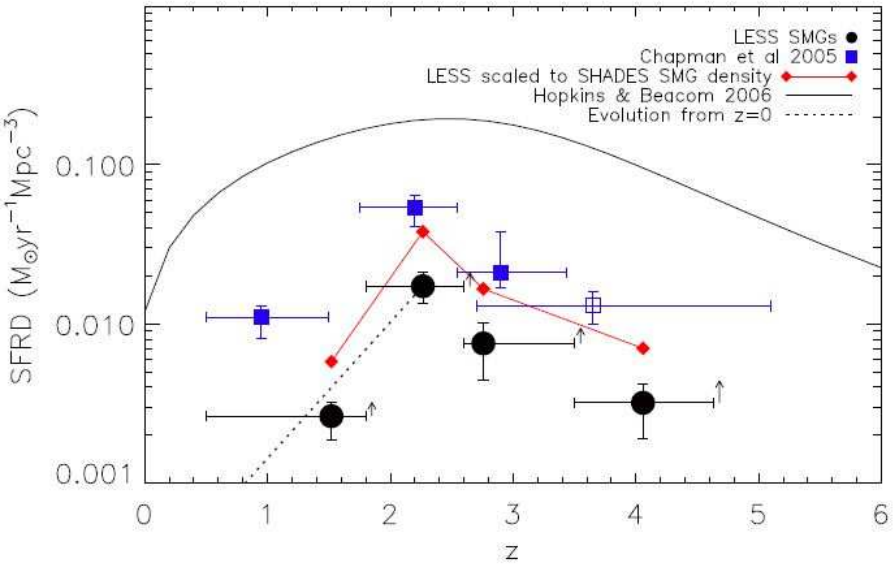

Figure 5.2 From Wardlow et al. (2011). Evolution of the SFRD for the radio-detected LESS SMGs compared to Chapman et al. (2005)). Arrows to the right of each LESS redshift bin indicate the maximum additional contribution from unidentified SMGs and the open symbol represents unidentified SMGs from Chapman et al. (2005)). The LESS SMG activity peaks at $z \sim 2$. The contribution from SMGs to the total SFRD also peaks at $z \sim 2$ where they are responsible for $\sim 10\%$ of the SFRD.

them the measured redshift distribution and assuming radio fluxes equal to the detection limit. The calculated SFRD of the unidentified SMGs from this analysis is an upper limit since the actual radio fluxes will typically be lower than the detection limit. The SFRD of the LESS SMGs appears to peak at $z \sim 2$, similar to Chapman et al. (2005); even though the LESS SMGs have a lower SFRD, the lower number density of SMGs in the ECDFS is sufficient to account for this effect. The fractional contribution of LESS SMGs to the SFRD of the Universe also peaks at $z \sim 2$ where they are responsible for $\sim 10\%$ of the SFRD. The median SFR is $1100 \pm 100\, M_{\odot}\, year^{-1}$, but caution is needed due to the uncertainties in the stellar mass estimates that can bring additional factor of ~ 5 uncertainty in these values. The median formation timescale of the LESS SMGs is thus $\sim 100\, Myr$.

5.2 Latest results - ALMA

The latest instrument that replaced SCUBA in matter of importance and sensitivity was its successor, SCUBA-2 (see Holland et al. (2013)). This 10000 pixel bolometer camera has been in use on the JCMTT since 2012, and has the capability to carry out wide-field surveys to far better depths than its older sibling. It has two imaging arrays working simultaneously at $450\,\mu m$ and $850\,\mu m$, thus allowing a dramatic increase in pixel count, mapping the sky 100-150 times faster than before and covering much larger areas. The latest and widest survey carried out with SCUBA-2 is the Cosmology Legacy Survey (CLS), which provided a catalogue of ~ 3000 submillimetre sources detected ($\geq 3.5\sigma$) at $850\,\mu m$ over $\sim 5\, deg^2$, making it the largest survey of its kind at this wavelength, increasing the sample size of $850\,\mu m$ selected submillimetre galaxies by an order of magnitude. It covers the extragalactic fields: UKIDSS-UDS, COSMOS, Akari-NEP, Extended Groth Strip, Lockman Hole North, SSA22 and GOODS-North, thus allowing a very good study of cosmic variance.

The real revolution in the field, however, was the Atacama Large Millimeter Array (ALMA): in fact, the main flaw of single-dish observations was their low angular resolution ($\sim 15" - 20"\ FWHM$), resulting in a high difficulty in identifying multiwavelength counterparts with fair robustness. The use of an array like ALMA, composed of 66 high-precision antennas, allowed carrying out surveys with unprecedented depth and precision, paving the way for radioastronomy to become one of the most important tools to explore distant Universe. Many surveys were carried out during several cycles of observations; one of the very first was presented by Hodge et al. (2013): it consists in the observation of 126 submillimeter sources from the LABOCA ECDFS Submillimeter Survey (LESS) at $870\,\mu m$ made with ALMA (ALESS), that produced maps $\sim 3x$ deeper and with a beam area $\sim 200x$ smaller than the original LESS observations, allowing to pre-

cisely locate the origin of the submillimeter emission from the SMGs. The main improvement that differentiates ALMA data from previous studies is that the former precisely locate the SMGs, directly pinpointing the sources responsible for the submm emission (to within < 0.3"), without using statistical radio/MIR associations and thus yielding unambiguous identifications for the majority of the SMGs. These observations made ALESS the first statistically reliable survey of SMGs, which allowed for a complete and unbiased multi-wavelength study of the properties of this galaxy population. Identifying and extracting sources from the final maps, they recovered 99% of all SMGs above 3.5σ with a spurious fraction of 1.6%. From the analysis of the inverted maps, they estimated that 75%/90% of SMGs above $3.5\sigma/4\sigma$ may be regarded as reliable, though these estimates should be considered as lower limits. They also found a consistent fraction of the sample (about 35/40%, up to an upper limit of 50%) to be multi-component objects. Furthermore, 17 out of 88 good-quality maps ($\sim 20\%$) have no detected SMGs, even though only ~ 3.5 of the LESS sources are expected to be spurious. It may be that the emission from these LESS sources has been spread out into diffuse or multicomponent morphologies below their detection threshold. Finally, as for the completeness of the catalogue, considering only robust counterparts, the radio/midinfrared identification process has a completeness of only $\sim 45\%$, but a reliability of $\sim 80\%$: although being it only an initial study, their results in terms of reliability are very encouraging. A study on the physical properties of this sample of SMGs was made by Swinbank et al. (2014). They use the precisely located positions of 99 SMGs, together with $24\,\mu m$ and radio imaging of the Extended Chandra Deep Field South, deblending the Herschel / SPIRE imaging of this region to extract their far-infrared fluxes and colours. In particular, they used the far-infrared ($70-870\,\mu m$) and 1.4GHz radio photometry together with new optical/mid-infrared-derived photometric redshifts to derive the far-infrared luminosities, characteristic dust temperatures, dust masses and their evolution with redshift. However, our review will cover only the results regarding the SFRD, for more details see Swinbank et al. (2014). They used photometric redshifts for the 96 ALESS SMGs to derive a rest-frame UV-radio composite SED for the whole sample; then, using the best-fit dust SEDs, they calculated the infrared luminosity (L_{IR}) by integrating the rest-frame SED between $8 - 1000\,\mu m$. Using the photometric redshift distribution for the ALESS SMGs, they showed that the dust SEDs for the SMGs that peak at shorter wavelengths lie at the lower redshifts, whilst those which peak at the longer wavelengths lie at the highest redshifts: in fact, the dust SEDs that peak closest to 250, 350 and $500\,\mu m$ peak at $z = 2.3 \pm 0.2$, 2.5 ± 0.3 and 3.5 ± 0.5 respectively. However, there are 34 (out of 99) ALESS SMGs which do not have a $> 3\sigma$ counterpart at 250, 350 or $500\,\mu m$. Of these 34 galaxies, 30 are also radio unidentified; carrying out the same analysis for this subsample only, it is interesting to note that the median photometric redshift for these

SPIRE and radio non-detections is higher than the full ALESS SMG sample, thus revealing how they represent a combination of the slightly fainter and higher redshift subset of the ALESS SMGs. The median infrared luminosity for the complete sample of ALESS SMGs is $L_{IR} = (3.0 \pm 0.3) * 10^{12}\, L_{\odot}$ (corresponding to $SFR = 310 \pm 30\, M_{\odot}\, yr^{-1}$ for a Chabrier IMF) with a range of $L_{IR} = (0.2 - 10) * 10^{12}\, L_{\odot}$ ($SFR = 20 - 1030 \pm 30\, M_{\odot}\, yr^{-1}$). This is a factor $\sim 1.8x$ lower than that derived by Chapman et al. (2005). However, this is mainly driven by the high multiplicity of SMGs due to unresolved companions in the far-infrared photometry in the single-dish survey, as already stated by the work from Hodge et al. (2013). In order to derive the luminosity functions, they adopted the usual V_{max} method; then, they inferred the SFRD. The results are shown in Figure 5.3.

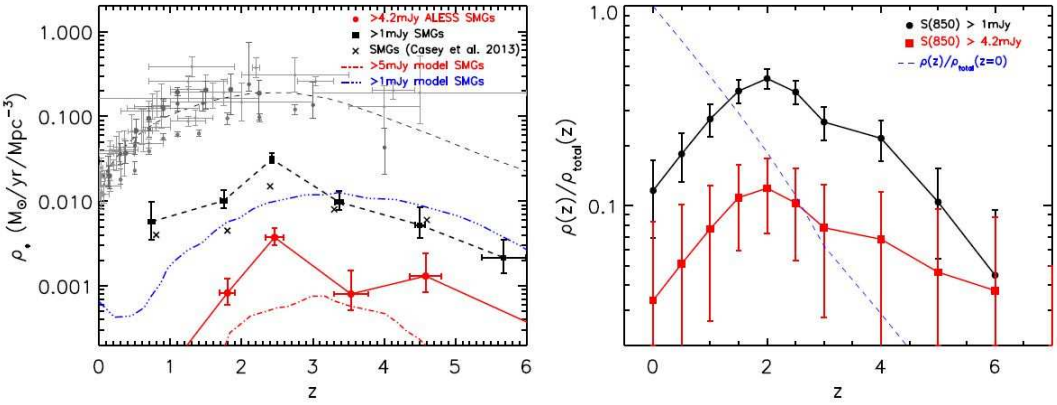

Figure 5.3 From Swinbank et al. (2014). *Left panel*: The contribution of SMGs to the co-moving cosmic star formation density as a function of redshift. Since the original LESS survey had flux density limits of $S_{870\,\mu m} = 4.2\, mJy$, they only included ALESS SMGs brighter this limit, but then extrapolated to all SMGs brighter then $S_{870\,\mu m} = 1\, mJy$ using the $850\,\mu m$ data. This plot shows that the SMG activity peaks at $z \sim 2$ - similar to that found by previous studies of star-forming galaxies and the peak activity of QSOs. The contribution from bright SMGs to the total SFRD also peaks at $z \sim 2$ where they are responsible for $\sim 12\%$ of the SFRD, although extrapolating to the faintest SMGs, $\sim 1\, mJy$ data suggest that SMGs contribute up to 20% of the total SFRD at this epoch. *Right panel*: Fraction of stellar mass in SMGs ($S_{870\,\mu m} > 4.2\, mJy$) compared to the total stellar mass density as a function of redshift. This figure shows that at $z \gtrsim 2 - 3$ the bright SMGs ($S_{870\,\mu m} > 4.2\, mJy$) contribute to $\sim 15\%$ of the total stellar mass budget at that epoch, and make up 34% of the present day stellar mass density. Integrating to fainter luminosities as before, SMGs are predicted to contribute to $\sim 30 - 40\%$ of the comoving stellar mass density at $z \sim 2$.

When calculating the star formation rate density, they included all of the SMGs from the ALESS main catalogue with $S_{870\,\mu m} > 4.2\,mJy$ (the flux limit of the original LESS survey), and accounted for a factor $2x$ in under-density of SMGs in the ECDFS. As Figure 5.3 shows, over the redshift range $z = 1 - 5$, bright SMGs account for $\sim 12\%$ of the total star formation density. However, accounting for the large fraction of the sub-millimeter galaxy population below their flux limit, they integrated down to $1\,mJy$. This flux represents the point at which the dust-obscured and unobscured star formation rates in galaxies are comparable and corresponds to an infrared luminosity of $L_{IR} = (0.8) * 10^{12}\,L_{\odot}$ ($SFR = 80\,M_{\odot}\,yr^{-1}$). Assuming that the fainter SMGs ($S_{870\,\mu m} = 1 - 4.2\,mJy$) have the same underlying redshift distribution and luminosity evolution as the bright ones, they found that the number density of faint SMGs is $7x$ that of those bright. This yields a SMGs contribution to the total star formation over the redshift range $z = 1 - 5$ of $\sim 20\%$. However, this value is to be considered a lower limit, since they have not included ULIRGs which have comparable luminosities as the SMGs but with hotter than average dust temperatures which makes them fainter at $870\,\mu m$, dropping them below the LESS flux limit. These may increase the contribution to the star formation rate density by a factor $\lesssim 2x$ compared to the $870\,\mu m$-only selection. They also measured the fraction of stellar mass in SMGs compared to the total comoving stellar mass density (as a function of redshift), as depicted in Figure 3.5. Assuming the SMGs have a burst duration of $250\,Myr$, they found that at $z \sim 2 - 3$, the bright SMGs ($S_{870\mu m} \geq 1 - 4.2\,mJy$) contribute to a 15% of the total comoving stellar mass density at this epoch. In contrast, by $z = 0$ the plot suggests that the total stellar mass formed in bright SMGs comprises just $\sim 34\%$ of the total stellar mass density. Integrating for fainter sources as above, SMGs account for $30 - 40\%$ of the total stellar mass at $z \sim 2$, and $\sim 15\%$ of the total comoving stellar mass density at $z = 0$.

Another important ALMA survey was carried out in the COSMOS field, which has an exceptional coverage of multiwavelength data, as seen, with results reported by Miettinen et al. (2017). The target SMGs were originally identified by the $\lambda_{obs} = 1.1\,mm$ blank-field continuum survey over a continuous area of $0.72\,deg^2$ COSMOS field carried out with the 144 pixel AzTEC bolometer camera. The 129 brightest AzTEC sources were followed up with dedicated ALMA pointings at $\lambda_{obs} = 1.3\,mm$ and $\sim 1".6x0".9$ angular resolution with a 1σ root-mean-square (rms) noise of $\sim 0.1\,mJy\,beam^{-1}$. 33 were resolved into two or three components, and in total they detected 152 ALMA sources at an $S/N_{1.3\,mm} \geq 5$ ($S^{ALMA}_{1.3\,mm} \gtrsim 0.5\,mJy$). This yields a sample that is expected to be free of spurious sources, i.e. the sample reliability reaches a value of $\sim 100\%$. The ALMA follow-up survey allowed to accurately pin down the positions of the single-dish AzTEC sources. For details on AGN removal and counterparts matching, see Miettinen et al. (2017). The SEDs of the sample are constructed using the MAGPHYS code, which

is built on a global energy balance between stellar and dust emissions but has the potential caveat that the visible (unobscured) stellar component can be spatially decoupled from the dust-emitting, obscured star-forming parts, in which case the UV-optical and far-IR to mm photometry might not be coupled in the way assumed in the SED modelling. Starting from these data, they derived L_{IR} as a function of redshift, with a best-fit function that has the form of $log(L_{IR}/L_{\odot}) = (11.3 \pm 0.2) * (1+z)^{0.09\pm0.01}$. This apparent behaviour of increasing L_{IR} with z is a well-known selection effect: $z \gtrsim 3$ SMGs are likely biased towards warmer objects than at lower redshifts, characterised by luminosity-weighted dust temperatures of $T_{dust} \lesssim 50\,K$ at $z \gtrsim 3$. From these data IRLFs and SFRs are calculated for the entire sample, through the already mentioned MAGPHYS code.
In Figure 5.4 they plot the L_{IR}-based SFR values of the SMGs as a function of their stellar mass. The tight and almost linear correlation between the SFR and M_* is the so-called main-sequence (MS) of star-forming galaxies and and it provides valuable insight into how galaxies convert their gaseous ISM into stars.

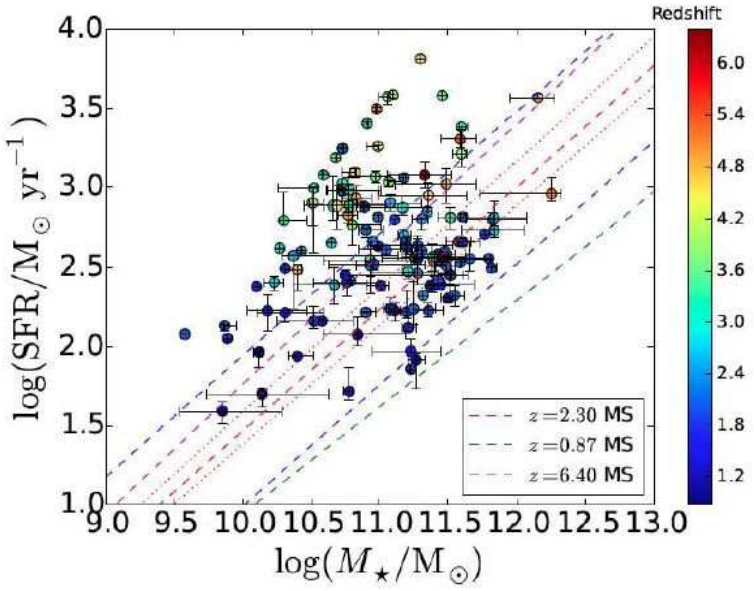

Figure 5.4 From Miettinen et al. (2017). Main sequence diagram for these ALMA SMGs (a log-log plot of the SFR versus stellar mass). The data points are colour-coded with redshift as shown in the colour-bar on the right. The red dashed line shows the mid-line position of the star-forming MS at the median redshift of the analysed SMGs ($z = 2.30$), with the lower and upper blue dashed lines indicating a factor of three offset below and above the MS.

This value has a best-fit analytical form derived from a compilation of 25 observational studies out to $z \sim 6$ with different pre-selections (UV, optical, far-IR), and is given by:

$$log(SFR/M_{\odot}\, yr^{-1}) = (0.84 - 0.026\tau_{univ})log(M_*/M_{\odot}) - (6.51 - 0.11\tau_{univ})$$

where τ_{univ} is the age of the universe in Gyr: this equation gives the locus of the MS. Hence, the MS evolves with redshift by shifting to higher SFRs at earlier cosmic times. In order to quantify the offset from the MS mid-line, they calculated the ratio of the derived SFR to that expected for a MS galaxy of the same redshift and M_*, that is $\Delta_{MS} = SFR/SFR_{MS}$. 52 out of the 124 SMGs ($\sim 41.9\%$) analyzed here lie above the $\Delta_{MS} = 3$ border. These sources are defined as starbursts; 71 of our SMGs ($\sim 57.3\%$) instead lie within the MS. So, some of the SMGs are found to be located on or close to the MS (at the high-M_* end), while a fair percentage of SMGs, especially the most luminous objects, are found to lie above the MS: this yields a view where SMG populations exhibit two different types of star formation modes, namely a steady conversion of gas into stars as in normal (non-starburst) star-forming disk galaxies, and star formation in more violent, bursty event, which is likely triggered by major mergers.

In Figure 5.5, they plotted the sSFR, which reflects the strength of the current star formation activity with respect to the underlying galaxy stellar mass, as a function of redshift. The sSFR appears to increase as a function of redshift from $z \sim 1$ to $z \sim 3$ and then showing a plateau at $z \gtrsim 3$.

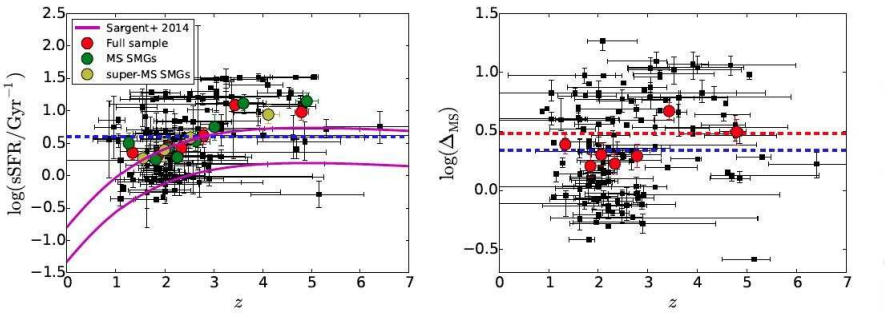

Figure 5.5 From Miettinen et al. (2017). Specific SFR (sSFR; *left panel*) and starburstiness (*right panel*) as a function of redshift. The red filled circles represent the mean values of the binned data for the full sample. In the left panel, the green and yellow filled circles represent the mean values of the binned data for the MS SMGs and starburst SMGs, respectively. The blue horizontal dashed lines mark the sample median values of $sSFR = 3.9\, Gyr^{-1}$ and $\Delta_{MS} = 2.2$.

A positive sSFR(z) evolution is likely to reflect the higher molecular gas masses and densities at earlier cosmic times, which regulates the physics underlying star-formation activity. The plot with the starburstiness as a function of redshift shows an average behaviour similar to that seen in the left panel, where the sSFR represents the normalisation of the MS at a given stellar mass, while the Δ_{MS} in the right panel is the offset from the MS mid-line. They also carried on a deep analysis on how the dust and gas mass contents of the SMGs are related with their SFR, and on possible dependencies of the SFR, Δ_{MS}, and T_{dust} on the radio-emitting sizes of the SMGs, but this is beyond the purpose of this thesis. It is important to stress that less than half ($42\% \pm 6\%$) of the SMGs appear to lie above the MS (by a factor of greater than three), and can be considered starbursts. The remainder of the sample appears to be composed of highly star-forming MS galaxies. Considering the sample and the L_{IR} selection effect that it is subject to, the dividing IR luminosity limit between MS SMGs and starburst SMGs is $L_{IR} \sim 9 * 10^{12}\, L_{\odot}$. The IR-based SFRs of the super-MS, starburst SMGs are $\sim 39 - 6500\, M_{\odot}\, yr^{-1}$ with a median of $767\, M_{\odot}\, yr^{-1}$, while those for the MS SMGs were derived to be $\sim 50 - 3700\, M_{\odot}\, yr^{-1}$ with a median of $\sim 346\, M_{\odot}\, yr^{-1}$. Clearly, the star formation activity is very intense in the MS SMGs as well. The aforementioned very high SFRs could be triggered by gas-rich galaxy mergers or by gravitational instabilities in very gas-rich galaxies for which the gas supply is maintained by continuous, cold gas accretion; the MS SMGs appear to exhaust their molecular gas reservoir through star formation slower on average than the starburst objects from the analysis of the correlation of gas and stellar content (Miettinen et al. (2017)). The authors also found that the SMGs that are classified as irregulars in the rest-frame UV appear to be predominantly starbursts, while those classified as disks are mostly found within the MS. They interpreted this as an evidence of irregulars being merger systems where high-mass stars are being formed at a rapid rate. The emerging scenario from this data is as follows: $z > 3$ SMGs quench into very compact, spheroid-like galaxies found at $z \sim 2$, and hence SMGs at $z > 3$ are unlikely to evolve into a single class of galaxies by $z \sim 2$. This conclusion is based on the mass-size relationship analysis, which however is hampered by the uncertainties in the sizes of SMGs as seen at different wavelengths. More accurate gas masses are needed to better understand the expected final stellar masses of the $z > 3$ SMGs, and how those compare with the masses of $z \sim 2$ cQGs. Another obvious caveat here is the spectroscopical confirmation that is missing for most sources. On the other hand, it seems possible that the $z \sim 2$ cQGs evolved from compact SFGs rather than from more extreme SMGs. Their results did not support the view that these three types of galaxies would form an evolutionary sequence. Instead, they agreed best with the scenario where the highest redshift ($z \gtrsim 4$) SMGs quench their spatially compact star formation, and evolve into quiescent systems found at high redshifts

($z \gtrsim 3$). Regarding the $z \lesssim 3$ SMGs, they found some supporting evidence on the basis of their estimated stellar mass growth that they might form the ultra-massive, dense ellipticals seen at $z < 2$.

Chapter 6

Conclusions and future prospects

This thesis has reviewed the state of the art in matter of star-formation history in a fashion that aimed to give a complete and thorough view on the subject. We have seen the different tracers of star-formation and their respective flaws: UV light, that directly traces SF accounting for the presence of young stars but is severely affected by dust extinction, thus depending on absorption laws that are often inaccurate; furthermore, it does not take into account the presence of redder populations that form the bulk of the mass in a galaxy. IR light, originated from the re-emission of UV light absorbed by dust, accounts for what is missing from UV light, but not all sources are affected by this problem; furthermore, other sources not connected to SFR processes may contaminate the emission, and dust spectrum can be very complicated. Radio light has the great credit of being immune to dust effects, thus allowing to reach very high redshift, but needs accurate analyses because of the presence of AGNs that contaminate the samples and for the difficulty of matching multiwavelength counterparts, crucial factor in deriving the physical properties of a population; furthermore, the link between radio emission and star formation is still not well understood, for it encloses electron acceleration by SNe explosions and black holes, and the parameter that controls this correlation still needs future corrections. We have seen how the choice for the IMF is crucial: it affects deeply the SFRD estimates because it controls the evolution (both in luminosity and colour) of a stellar population, so one must be very careful in analyzing the data and not underestimating the influence of this parameter. It controls the conversion factor that enables the estimate of the SFR from the total luminosity of a wavelength range (namely, UV or IR). Another important factor that influences the SFRD estimate is the luminosity function: wide and deep data are needed to constrain both the bright- and the faint- end slope of the function, but such data needs betterment and future astronomical tools will

surely help in the matter.

Madau & Dickinson (2014) found that their SFH peaked around $z \sim 1.5 - 2$ with a rising phase at higher redshifts and a declining one towards today; the problem with their work was that the relative SMD was over-predicted in comparison with most of the literature. We saw how the problem probably relies in the choice of a Salpeter IMF: in fact, Franceschini et al. (2014) carried out a similar analysis with robust IR data choosing the Chabrier IMF, that converges in shallower slopes at stellar massed $< 1\,M_{\odot}$, and finding a SFH that peaks around $z \sim 0.8 - 1.2$ and then has a plateau out to $z \sim 3$.

Concerning radio emission, a deep and thourough digression on AGN classification and methods to identify them has been made. After that, we presented the most important result from Novak et al. (2017), who derived a SFRD that agrees very well with previous IR estimates and has a deep difference with the Madau one, coming from the already-cited IMF problem. So, there appears to be a fair consensus on the subject. Furthermore, the IR-radio correlation has been thoroughly analyzed, its evolution with the redshifts an the problems related to its derivation.

Lastly, submillimeter emission has been reviewed: it traces ultra-luminous and very dusty galaxies at high redshift, whose luminosity peaks in the submm wavelengths and are hardly detectable in the radio range of the spectrum. Robustly pinpointed and high resolution data needs interferometer observations to be derived: ALMA suits this task perfectly. Both Swinbank et al. (2014) and Miettinen et al. (2017) found SFRD values that are similar to the previous literature, but they made a step forward in their analysis by estimating the relative influence of this galaxy population in the total SMD budget at various epochs. They estimated a lower limit for SMGs contribution to the star-formation rate density of $\sim 20\%$ in the redshift range $z = 1 - 5$. Furthermore, their contribution to the total stellar mass budget increases with redshift, suggesting that SMGs could be the progenitors of the present-day giant elliptical and/or QSOs. In fact, a large percentage of this galaxy population appears to lie above the main sequence of star-formation, thus being considered starburst objects, maybe gaseous galaxy mergers systems with very high star-formation rate values.

SFRD estimates will surely be bettered with the upcoming surveys and facilities that will pave the way for an unprecedented evolution in cosmology. In radioastronomy, instruments like the Square Kilometre Array (SKA - with a total collecting area of approximately $1\,km^2$ and a sensitivity 50x larger than any other present instruments) and the Next Generation Very Large Array (ngVLA- with 10x the collecting area of the Jansky VLA & ALMA and science operations from 1.2 - 116 GHz) will provide unprecedented sensitive data; radio data will need to be coupled with multiwavelength ones, and upcoming facilities like The Large Synoptic Survey Telescope (LSST) and Euclid will provide such data.

Bibliography

Arnouts, S., Schiminovich, D., Ilbert, O., et al. 2005, ApJ, 619, L43

Butler, A., Huynh, M., Delhaize, J., et al. 2017, ArXiv e-prints

Chapman, S. C., Blain, A. W., Smail, I., & Ivison, R. J. 2005, ApJ, 622, 772

Conroy, C., Gunn, J. E., & White, M. 2009, ApJ, 699, 486

Coppin, K., Chapin, E. L., Mortier, A. M. J., et al. 2006, MNRAS, 372, 1621

Cucciati, O., De Lucia, G., Zucca, E., et al. 2012, A&A, 548, A108

Delhaize, J., Smolčić, V., Delvecchio, I., et al. 2017a, A&A, 602, A4

Delhaize, J., Smolčić, V., Delvecchio, I., et al. 2017b, A&A, 602, A4

Elbaz, D., Cesarsky, C. J., Chanial, P., et al. 2002, A&A, 384, 848

Franceschini, A., Aussel, H., Cesarsky, C. J., Elbaz, D., & Fadda, D. 2001, A&A, 378, 1

Franceschini, A., Marchetti, L., & Rodighiero, G. 2014

Gallazzi, A., Brinchmann, J., Charlot, S., & White, S. D. M. 2008, MNRAS, 383, 1439

Geach, J. E., Dunlop, J. S., Halpern, M., et al. 2017, MNRAS, 465, 1789

Gruppioni, C., Pozzi, F., Rodighiero, G., et al. 2013, MNRAS, 432, 23

Hodge, J. A., Karim, A., Smail, I., et al. 2013, ApJ, 768, 91

Holland, W. S., Bintley, D., Chapin, E. L., et al. 2013, MNRAS, 430, 2513

Ivison, R. J., Greve, T. R., Dunlop, J. S., et al. 2007, MNRAS, 380, 199

Laigle, C., McCracken, H. J., Ilbert, O., et al. 2016, ApJS, 224, 24

Lawrence, A., Walker, D., Rowan-Robinson, M., Leech, K. J., & Penston, M. V. 1986, MNRAS, 219, 687

Le Floc'h, E., Papovich, C., Dole, H., et al. 2005, ApJ, 632, 169

Lilly, S. J., Tresse, L., Hammer, F., Crampton, D., & Le Fevre, O. 1995, ApJ, 455, 108

Madau, P. 1998, in Structure et Evolution du Milieu Inter-Galactique Revele par Raies D'Absorption dans le Spectre des Quasars, 13th Colloque d'Astrophysique de l'Institut d'Astrophysique de Paris, ed. P. Petitjean & S. Charlot, 295

Madau, P. & Dickinson, M. 2014, ARA&A, 52, 415

Madau, P., Ferguson, H. C., Dickinson, M. E., et al. 1996, MNRAS, 283, 1388

Miettinen, O., Delvecchio, I., Smolčić, V., et al. 2017, A&A, 606, A17

Novak, M., Smolčić, V., Delhaize, J., et al. 2017, A&A, 602, A5

Reddy, N. A., Steidel, C. C., Pettini, M., et al. 2008, ApJS, 175, 48

Rodighiero, G., Cimatti, A., Gruppioni, C., et al. 2010, A&A, 518, L25

Salpeter, E. E. 1955, ApJ, 121, 161

Sanders, D. B., Mazzarella, J. M., Kim, D.-C., Surace, J. A., & Soifer, B. T. 2003, AJ, 126, 1607

Schiminovich, D., Ilbert, O., Arnouts, S., et al. 2005, ApJ, 619, L47

Schinnerer, E., Carilli, C. L., Scoville, N. Z., & COSMOS/VLA-COSMOS Collaboration. 2004, in Bulletin of the American Astronomical Society, Vol. 36, American Astronomical Society Meeting Abstracts, 1468

Schuller, F., Menten, K. M., Contreras, Y., et al. 2009, A&A, 504, 415

Smolčić, V., Delvecchio, I., Zamorani, G., et al. 2017a, A&A, 602, A2

Smolčić, V., Novak, M., Delvecchio, I., et al. 2017b, A&A, 602, A6

Smolčić, V., Schinnerer, E., Zamorani, G., et al. 2009, ApJ, 690, 610

Swinbank, A. M., Simpson, J. M., Smail, I., et al. 2014, MNRAS, 438, 1267

Tacconi, L. J., Genzel, R., Smail, I., et al. 2008, ApJ, 680, 246

Wardlow, J. L., Smail, I., Coppin, K. E. K., et al. 2011, MNRAS, 415, 1479